



 Cite this: *RSC Adv.*, 2026, 16, 19379

Novel NHC-based Pd–PEPPSI complexes: synthesis, structural characterization by X-ray diffraction, biological properties, and catalytic performance in *N*-alkylation reactions

 Lamia Boubakri,^a S. Hassen,^b Nevin Gürbüz,^{cde} İsmail Özdemir,^{cde} Youssef Arfaoui,^b Anis Attour,^f Harald Kelm,^g Jamil Kraiem^h and Naceur Hamdi *^a

Herein, we describe the borrowing-hydrogen *N*-alkylation of amines with alcohols using Pd-PEPPSI-NHC complexes, representing the first example of this catalyst class applied to this transformation. For this purpose, six novel benzimidazolium chlorides and their corresponding PEPPSI-type (PEPPSI = pyridine-enhanced precatalyst preparation, stabilization and initiation) palladium complexes bearing NHC spectator ligands were synthesized and fully characterized using a range of spectroscopic techniques. Additional structural details were confirmed by single-crystal X-ray diffraction analysis of one of the complexes. All newly synthesized Pd–carbene complexes demonstrated significant catalytic activity toward the alkylation of aniline derivatives with aryl alcohols. Excellent results were obtained within 24 hours using only 2.5 mol% of catalyst, highlighting an efficient and promising approach for this type of reaction. In addition, the antimicrobial activities of PEPPSI-Pd(II)–N-heterocyclic carbene (NHC) complexes **3a–f** were evaluated against *Micrococcus luteus*, *Listeria monocytogenes*, *Salmonella typhimurium*, *Staphylococcus aureus*, *Candida albicans* and *Pseudomonas aeruginosa*. We emphasize that all palladium–NHC–PEPPSI complexes are efficient compounds against bacteria and fungi as potential antimicrobial agents. In addition, the anticancer activity of these compounds was determined. Higher cytotoxicity relative to cisplatin was observed across all tested cell lines.

 Received 6th January 2026
 Accepted 19th February 2026

DOI: 10.1039/d6ra00146g

rsc.li/rsc-advances

1 Introduction

The formation of carbon–nitrogen bonds is a cornerstone of modern organic synthesis, as alkylamines serve as essential scaffolds in pharmaceuticals, agrochemicals, dyes, and polymeric materials.^{1–3} Conventional *N*-alkylation strategies, including nucleophilic substitution of alkyl halides, reductive amination of carbonyl compounds, and transition-metal-

catalyzed hydroamination of alkenes or alkynes, are well established.^{4–6} However, these methods frequently face drawbacks such as low atom economy, only moderate selectivity, harsh reaction conditions, and the production of stoichiometric inorganic waste, which create notable environmental and economic concerns.⁷ In recent years, borrowing-hydrogen (hydrogen autotransfer) catalysis has emerged as a sustainable and atom-efficient alternative for *N*-alkylation reactions.^{8–10} This redox-neutral strategy uses alcohols as both the alkyl source and hydrogen donor. The process involves catalytic dehydrogenation of alcohol to a reactive carbonyl intermediate, which condenses with an amine to form an imine. The imine is subsequently reduced *in situ* by the hydrogen originally abstracted from the alcohol, producing the *N*-alkylated amine, with water as the only by-product (Scheme 1).^{11,12} This approach avoids external reducing agents and aligns with the principles of green chemistry. Borrowing-hydrogen *N*-alkylation of amines using alcohols is a well-established transformation and has been widely demonstrated with catalysts based on ruthenium, iridium, manganese, iron, and even palladium.^{13–17} Among transition metals, palladium catalysts are particularly attractive due to their versatile coordination chemistry, high redox activity, and extensive use in cross-coupling reactions.^{18–20} *N*-

^aResearch Laboratory of Environmental Sciences and Technologies (LR16ES09), Higher Institute of Environmental Sciences and Technology, University of Carthage, Hammam-Lif, Tunisia. E-mail: hamdi.naceur@isste.ucar.tn

^bLaboratory of Characterizations, Applications & Modeling of Materials (LR18ES08), Department of Chemistry, Faculty of Sciences of Tunis, University of Tunis El Manar, 2092, Tunisia

^cCatalysis Research and Application Center, İnönü University, 44280-Malatya, Turkey

^dDrug Application and Research Center, İnönü University, 44280-Malatya, Turkey

^eDepartment of Chemistry, Faculty of Science and Arts, İnönü University, 44280-Malatya, Turkey

^fChemical Engineering Department, College of Engineering, Imam Mohammad Ibn Saud Islamic University (IMSIU), Riyadh, 11432, Saudi Arabia

^gDepartment of Chemistry, RPTU Kaiserslautern-Landau, Erwin-Schrödinger-Str. Geb. 54, 67663 Kaiserslautern, Germany

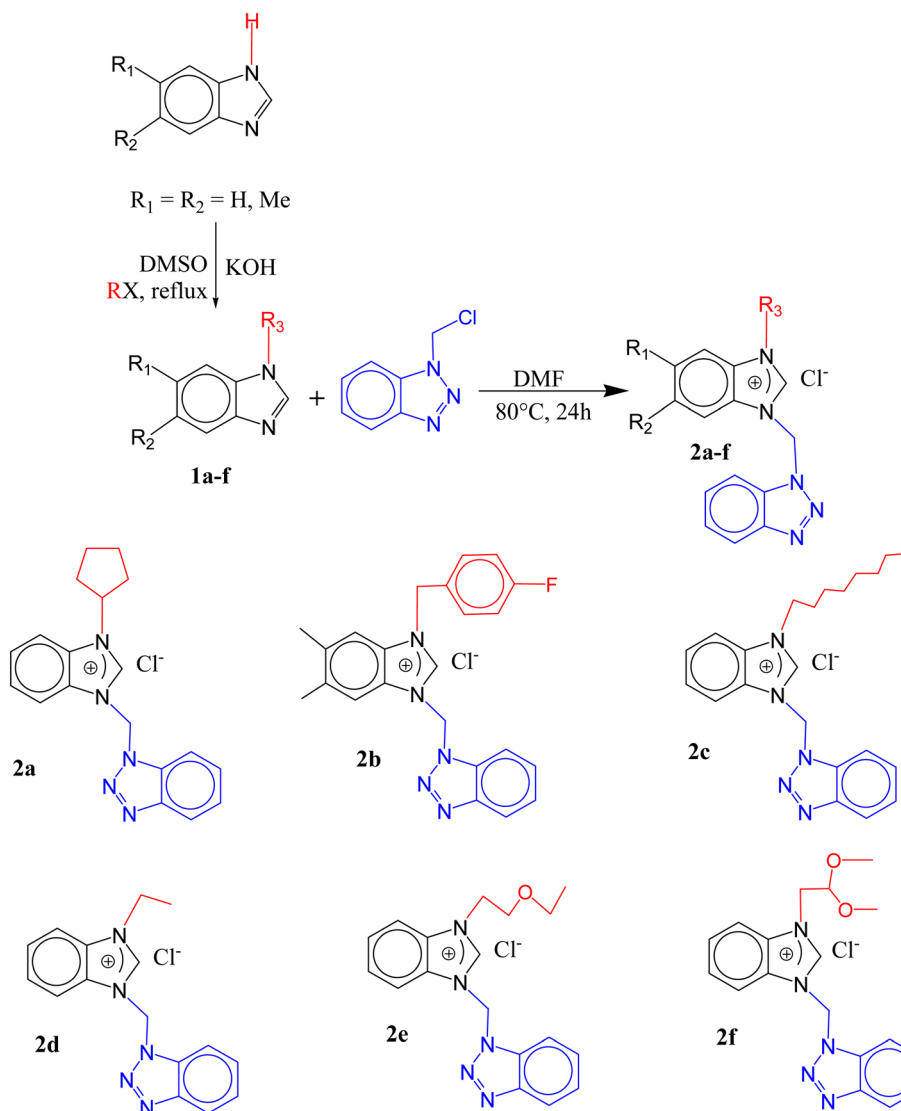
^hLaboratoire de Développement Chimique, Galénique et Pharmacologique des Médicaments, LR12ES09, Université de Monastir, Faculté de Pharmacie, Tunisia



Heterocyclic carbene (NHC) ligands have revolutionized palladium catalysis by providing strong σ -donation, steric tunability, and stabilization of the metal center.^{21–23} In this context, Pd-PEPPSI (pyridine-enhanced precatalyst preparation, stabilization, and initiation) complexes represent a major breakthrough. Introduced in 2006, these precatalysts feature a halide-bound palladium stabilized by an NHC ligand and a labile pyridine, combining air- and moisture-stability with ease of activation through pyridine dissociation.^{24–27}

While Pd-PEPPSI complexes have been extensively explored in cross-coupling reactions such as Suzuki–Miyaura, Mizoroki–Heck, and Sonogashira,^{28–30} their use in borrowing-hydrogen *N*-alkylation of amines has not been reported. In this work, we present the first application of specifically designed Pd-PEPPSI–NHC complexes in *N*-alkylation of amines with alcohol derivatives. Its novelty arises from the unique steric and electronic environment provided by the NHC ligands within the PEPPSI framework, which can improve catalytic efficiency, selectivity, and operational simplicity under mild, solvent-free

conditions.^{31–34} In addition to their catalytic properties, Pd–NHC and Pd–PEPPSI complexes exhibit notable biological activities, including antimicrobial, antifungal, and anticancer effects.^{35–38} The steric and electronic design of the NHC ligands can influence interactions with cellular targets, DNA, and enzymes, highlighting the potential for dual-functional complexes that combine catalytic and biological activity. Motivated by these opportunities, we report herein the design and synthesis of novel NHC-based Pd–PEPPSI complexes, their structural characterization *via* single-crystal X-ray diffraction, and a detailed evaluation of their catalytic performance in borrowing-hydrogen *N*-alkylation reactions using alcohols under solvent-free conditions. Furthermore, the biological properties of these complexes were examined to assess their potential as multifunctional systems. This study thus bridges sustainable catalytic methodology with biologically relevant Pd–NHC chemistry, providing a platform for the development of dual-functional metal complexes.



Scheme 1 Synthesis of benzimidazolium chlorides 2a–f.



2 Experimental

2.1 Materials and measurements

All procedures were performed under an inert atmosphere using standard Schlenk line techniques. Chemicals and solvents were purchased from Sigma-Aldrich (Istanbul, Turkey). Solvents and liquid reagents were distilled under nitrogen. Open capillary tubes were used in an Electrothermal 9200 melting-point apparatus to analyze the melting points of the synthesized compounds. For FT-IR examination, a PerkinElmer Spectrum 100 spectrometer was used, which has a range from 4000 to 400 cm^{-1} . NMR spectra of the compounds were recorded with a Bruker Ascend™ 400 Avance III HD working at 400 MHz (^1H) and 100 MHz (^{13}C). NMR measurements were conducted in high-quality 5 mm NMR tubes in CDCl_3 and DMSO using tetramethylsilane (TMS, $\delta = 0.00$ ppm) as an internal standard. Chemical shifts (δ) are reported in parts per million (ppm) downfield from TMS. Multiplicities are designated as: s = singlet, d = doublet, t = triplet, m = multiplet. To measure catalytic activity (conversion and yield), a Shimadzu GC 2025 with a GC-FID sensor and an RX-5 ms column (30 m length, 0.25 mm diameter and 0.25 μm film thickness) was used. Column chromatography was performed using silica gel 60 (70–230 mesh). All the measurements were taken at room temperature using freshly prepared solutions.

2.2 General procedure for the preparation of *N*-alkylbenzimidazole derivatives (1a–f)

N-alkylbenzimidazole and *N*-alkyl-5,6-dimethylbenzimidazole were synthesized by reacting the corresponding unsubstituted benzimidazole derivatives (2 mmol) with potassium hydroxide (4.5 mmol) in DMSO. The mixture was stirred at 50 °C for 24 h, after which the appropriate aryl halide (2.1 mmol) was added dropwise. The reaction mixture was then refluxed for 3 days. Upon cooling to room temperature, water was added, and the resulting residue was extracted with 30 mL of dichloromethane. The organic layer was filtered and concentrated under reduced pressure. The obtained product was dried under vacuum and characterized by NMR spectroscopy.

2.2.1 1-Cyclopentylbenzimidazole (1a). Yield: 66.42%, brown solid, mp: 49.9 °C. FT-IR $\nu(\text{CN})$: 1483.33 cm^{-1} . ^1H NMR (400 MHz, CDCl_3), δ (ppm): 1.81–1.84 (m, 2H, H_4 , C_5H_9), 1.91–1.94 (m, 2H, H_3 , C_5H_9), 2.04–2.07 (m, 2H, H_5 , C_5H_9), 2.25–2.29 (m, 2H, H_2 , C_5H_9), 4.72–4.76 (m, 1H, H_1 , C_5H_9), 7.27–7.30 (m, 2H, $\text{H}_{5,6}$, Ar-*H*), 7.43–7.45 (m, 1H, H_7 , Ar-*H*), 7.79–7.82 (d, 1H, H_4 , Ar-*H*), 7.96 (s, 1H, H_2 , NCHN). ^{13}C NMR (100 MHz, CDCl_3), δ (ppm): 23.89 ($\text{C}_{3,4}$, C_5H_9), 32.27 ($\text{C}_{2,5}$, C_5H_9), 57.01 (C_1 , C_5H_9), 110.34, 120.36, 122.05, 122.59, 133.78, 140.80 (Ar-*C*), 144.03 (C_2 , NCHN).

2.2.2 1-(4-Fluorobenzyl)-5,6-dimethylbenzimidazole (1b). Yield: 86.05%, yellow solid, mp: 120.9 °C. FT-IR $\nu(\text{CN})$: 1508.50 cm^{-1} . ^1H NMR (400 MHz, CDCl_3), δ (ppm): 2.34 (s, 3H, H_b , 5,6- $(\text{CH}_3)_2$ - C_6H_2), 2.36 (s, 3H, H_a , 5,6- $(\text{CH}_3)_2$ - C_6H_2), 5.28 (s, 2H, $\text{CH}_2\text{C}_6\text{H}_4(\text{F})$ -4), 7.00–7.02 (m, 2H, $\text{H}_{3,7}$, $\text{C}_6\text{H}_4(\text{F})$ -4), 7.04 (s, 1H, H_7 , Ar-*H*), 7.12–7.16 (m, 2H, $\text{H}_{4,6}$, $\text{C}_6\text{H}_4(\text{F})$ -4), 7.58 (s, 1H, H_4 , Ar-*H*), 7.82 (s, 1H, NCHN). ^{13}C NMR (100 MHz, CDCl_3), δ (ppm): 20.25 (5,6- $(\text{CH}_3)_2$ - C_6H_2), 20.59 (5,6- $(\text{CH}_3)_2$ - C_6H_2), 48.03

($\text{CH}_2\text{C}_6\text{H}_4(\text{F})$ -4), 110.01, 115.87, 116.09, 120.48, 128.64, 128.72, 131.32, 131.61, 132.42, 142.33, 142.63 (Ar-*C*), 161.26 (NCHN), 163.71 (Ar-*C*-F).

2.2.3 1-Octylbenzimidazole (1c). Yield: 88.66%, brown oil. FT-IR $\nu(\text{CN})$: 1495.54 cm^{-1} . ^1H NMR (400 MHz, CDCl_3), δ (ppm): 0.85 (t, 3H, H_{17} , C_8H_{15}), 1.22 (s, 6H, $\text{H}_{14,15,16}$, C_8H_{15}), 1.29 (s, 6H, $\text{H}_{11,12,13}$, C_8H_{15}), 4.11 (t, 2H, H_{10} , C_8H_{15}), 7.27–7.28 (m, 2H, $\text{H}_{5,6}$, Ar-*H*), 7.37 (d, 1H, H_7 , Ar-*H*), 7.79 (d, 1H, H_4 , Ar-*H*), 7.85 (s, 1H, NCHN). ^{13}C NMR (100 MHz, CDCl_3), δ (ppm): 14.10 (C_{17} , C_8H_{15}), 22.64 (C_{16} , C_8H_{15}), 26.86 (C_{15} , C_8H_{15}), 27.41 (C_{14} , C_8H_{15}), 29.14 (C_{13} , C_8H_{15}), 29.85 (C_{12} , C_8H_{15}), 31.77 (C_{11} , C_8H_{15}), 45.14 (C_{10} , C_8H_{15}), 109.72, 120.40, 122.03, 122.80, 133.87, 142.98 (Ar-*C*), 143.92 (NCHN).

2.2.4 1-Ethylbenzimidazole (1d). Yield: 87.84%, brown oil. FT-IR $\nu(\text{CN})$: 1490.04 cm^{-1} . ^1H NMR (400 MHz, CDCl_3), δ (ppm): 1.49–1.53 (t, 3H, H_{11} , C_2H_5), 4.16–4.22 (q, 2H, H_{10} , C_2H_5), 7.27–7.31 (m, 2H, $\text{H}_{5,6}$, Ar-*H*), 7.38–7.40 (d, 1H, H_7 , Ar-*H*), 7.80–7.82 (d, 1H, H_4 , Ar-*H*), 7.89 (s, 1H, NCHN). ^{13}C NMR (100 MHz, CDCl_3), δ (ppm): 15.26 (C_{11} , C_2H_5), 39.81 (C_{10} , C_2H_5), 109.58, 120.34, 122.00, 122.75, 133.60, 142.32 (Ar-*C*), 143.92 (NCHN).

2.2.5 1-(2-Ethoxyethyl)benzimidazole (1e). Yield: 91.7%, brown oil. FT-IR $\nu(\text{CN})$: 1483.34 cm^{-1} . ^1H NMR (400 MHz, CDCl_3), δ (ppm): 1.13 (t, 3H, H_{13} , OCH_2CH_3), 3.42 (q, 2H, H_{12} , OCH_2CH_3), 3.73 (t, 2H, H_{11} , $\text{NCH}_2\text{CH}_2\text{O}$), 4.30 (t, 2H, H_{10} , $\text{NCH}_2\text{CH}_2\text{O}$), 7.29 (m, 2H, $\text{H}_{5,6}$, Ar-*H*), 7.40 (d, 1H, H_7 , Ar-*H*), 7.81 (d, 1H, H_4 , Ar-*H*), 7.97 (s, 1H, NCHN). ^{13}C NMR (100 MHz, CDCl_3), δ (ppm): 15.40 (C_{13} , OCH_2CH_3), 45.48 (C_{12} , OCH_2CH_3), 67.20 (C_{11} , $\text{NCH}_2\text{CH}_2\text{O}$), 69.00 (C_{10} , $\text{NCH}_2\text{CH}_2\text{O}$), 109.93, 120.71, 122.36, 123.13, 134.27, 144.08 (Ar-*C*), 144.13 (NCHN).

2.2.6 1-(2,2-Dimethoxyethyl)benzimidazole (1f). Yield: 53.4%, white solid, mp: 90 °C. FT-IR $\nu(\text{CN})$: 1493.42 cm^{-1} . ^1H NMR (400 MHz, CDCl_3), δ (ppm): 3.32 (s, 6H, $\text{H}_{12,13}$, OCH_3), 4.18 (d, 2H, H_{10} , $\text{CH}_2\text{CH}(\text{OCH}_3)_2$), 4.51 (t, 1H, H_{11} , $\text{CH}_2\text{CH}(\text{OCH}_3)_2$), 7.25 (d, 2H, $\text{H}_{5,6}$, Ar-*H*), 7.56 (s, 1H, H_7 , Ar-*H*), 7.83 (s, 1H, NCHN). ^{13}C NMR (100 MHz, CDCl_3), δ (ppm): 47.44 (C_{10} , $\text{CH}_2\text{CH}(\text{OCH}_3)_2$), 55.08 ($\text{C}_{12,13}$, OCH_3), 102.71 (C_{11} , $\text{CH}_2\text{CH}(\text{OCH}_3)_2$), 109.53, 120.31, 122.12, 122.98, 134.06, 143.57 (Ar-*C*), 143.72 (NCHN).

2.3 General procedure for the preparation of the benzimidazolium chlorides (2a–f)

N-alkylbenzimidazole (1 mmol) or *N*-alkyl-5,6-dimethylbenzimidazole (1 mmol) was reacted with 1-(chloromethyl)benzotriazole (1.05 mmol) in DMF (5 mL) under continuous stirring at 80 °C for 24 h. In the case of NHC salt **2d**, *N*-octylbenzimidazole (1 mmol) was alkylated using 1-octyl chloride (1.05 mmol) in DMF (5 mL). This reaction mixture was initially stirred at room temperature for 5 h, followed by heating at 80 °C until completion. After completion of the reaction, the product either precipitated spontaneously or was induced to precipitate by the addition of diethyl ether. The resulting suspension was filtered under an inert atmosphere using a vacuum glass filter. The collected solid was washed with diethyl ether (3 \times 5 mL) and dried under reduced pressure. Final purification was achieved by recrystallization from a mixture of isopropanol and diethyl ether, affording the corresponding NHC salt as a pure solid.



2.3.1 1-Cyclopentyl-3-(1-methylbenzo-1,2,3-triazolyl) benzimidazolium chloride (2a). Yield: 100%, brown solid, mp: 234 °C. FT-IR $\nu(\text{CN})$: 1563 cm^{-1} . ^1H NMR (400 MHz, CDCl_3), δ (ppm): 1.83 (m, 2H, H_{13} , C_5H_9), 2.06 (m, 2H, H_{12} , C_5H_9), 7.24 (m, 2H, H_{14} , C_5H_9), 2.40 (m, 2H, H_{11} , C_5H_9), 4.92–5.26 (m, 1H, H_{10} , C_5H_9), 7.34–7.36 (m, 1H, H_{20} , Ar-H), 7.38 (s, 2H, H_{16} , $\text{CH}_2\text{-C}_6\text{H}_4\text{N}_3$), 7.60–7.69 (m, 2H, $\text{H}_{5,6}$, Ar-H), 7.93 (s, 2H, $\text{H}_{4,7}$, Ar-H), 7.96 (s, 2H, H_{19} , Ar-H), 8.40–8.42 (d, 1H, H_{18} , Ar-H), 8.94–8.96 (d, 1H, H_{21} , Ar-H), 12.52 (s, 1H, NCHN). ^{13}C NMR (100 MHz, CDCl_3), δ (ppm): 23.63 ($\text{C}_{12,13}$, C_5H_9), 32.39 ($\text{C}_{11,14}$, C_5H_9), 56.73 (C_{10} , C_5H_9), 60.52 (C_{15} , $\text{CH}_2\text{-C}_6\text{H}_4\text{N}_3$), 111.60, 113.45, 115.06, 119.78, 125.16, 127.64, 128.13, 129.65, 131.15, 131.28, 132.70, 142.31 (Ar-C), 145.91 (C_2 , NCHN).

2.3.2 1-(4-Fluorobenzyl)-3-(1-methylbenzo-1,2,3-triazolyl)-5,6-dimethylbenzimidazolium chloride (2b). Yield: 70.61%, white solid, mp: 235.4 °C. FT-IR $\nu(\text{CN})$: 1554 cm^{-1} . ^1H NMR (400 MHz, CDCl_3), δ (ppm): 2.33 (s, 3H, H_b , $(\text{CH}_3)_2\text{C}_6\text{H}_2$), 2.42 (s, 3H, H_a , $(\text{CH}_3)_2\text{C}_6\text{H}_2$), 5.72 (s, 2H, H_{10} , $\text{CH}_2\text{C}_6\text{H}_4\text{F}$), 7.02 (m, 2H, $\text{H}_{12,16}$, $\text{C}_6\text{H}_4\text{F}$), 7.23 (s, 1H, H_7 , $(\text{CH}_3)_2\text{C}_6\text{H}_2$), 7.39 (t, 1H, H_{23} , $\text{C}_6\text{H}_4\text{N}_3$), 7.46 (m, 2H, $\text{H}_{13,15}$, $\text{CH}_2\text{C}_6\text{H}_4\text{F}$), 7.62 (t, 1H, H_{22} , $\text{C}_6\text{H}_4\text{N}_3$), 7.86 (s, 2H, H_{17} , $\text{CH}_2\text{-C}_6\text{H}_4\text{N}_3$), 8.00 (d, 1H, H_{24} , $\text{C}_6\text{H}_4\text{N}_3$), 8.05 (s, 1H, H_4 , $(\text{CH}_3)_2\text{C}_6\text{H}_2$), 8.84 (d, 1H, H_{21} , $\text{C}_6\text{H}_4\text{N}_3$), 12.54 (s, 1H, NCHN). ^{13}C NMR (100 MHz, CDCl_3), δ (ppm): 20.75 ($\text{C}_{a,b}$, $(\text{CH}_3)_2\text{C}_6\text{H}_2$), 50.97 (C_{10} , $\text{CH}_2\text{C}_6\text{H}_4\text{F}$), 56.91 (C_{17} , $\text{CH}_2\text{-C}_6\text{H}_4\text{N}_3$), 111.25, 112.89, 114.22, 116.48, 116.70, 119.90, 125.19, 128.04, 129.35, 129.48, 129.62, 130.07, 130.15, 132.46, 138.27, 138.66 (Ar-C), 142.91 ($\text{C}_{14}\text{-F}$), 146.01 (C_2 , NCHN).

2.3.3 1-Octyl-3-(1-methylbenzo-1,2,3-triazolyl) benzimidazolium chloride (2c). Yield: 67.98%, purple solid, mp: 131.5 °C. FT-IR $\nu(\text{CN})$: 1560.03 cm^{-1} . ^1H NMR (400 MHz, $\text{DMSO-}d_6$), δ (ppm): 0.78 (M, 3H, H_{17} , C_8H_{17}), 1.17 (m, 6H, $\text{H}_{14,15,16}$, C_8H_{17}), 1.25 (m, 4H, $\text{H}_{12,13}$, C_8H_{17}), 1.89 (m, 2H, H_{11} , C_8H_{17}), 4.56 (t, 2H, H_{10} , C_8H_{17}), 7.45 (t, 1H, H_6 , C_6H_4), 7.64 (d, 1H, H_7 , C_6H_4), 7.68 (d, 1H, H_4 , C_6H_4), 7.74 (t, 1H, H_5 , C_6H_4), 7.87 (s, 2H, H_{18} , $\text{CH}_2\text{-C}_6\text{H}_4\text{N}_3$), 8.06 (d, 1H, H_{24} , $\text{C}_6\text{H}_4\text{N}_3$), 8.13 (d, 1H, H_{23} , $\text{C}_6\text{H}_4\text{N}_3$), 8.33 (d, 1H, H_{25} , $\text{C}_6\text{H}_4\text{N}_3$), 8.64 (d, 1H, H_{22} , $\text{C}_6\text{H}_4\text{N}_3$), 11.11 (s, 1H, NCHN). ^{13}C NMR (100 MHz, $\text{DMSO-}d_6$), δ (ppm): 13.82 (C_{17} , C_8H_{17}), 21.95 (C_{16} , C_8H_{17}), 25.67 (C_{15} , C_8H_{17}), 28.23–28.42 ($\text{C}_{12,13,14}$, C_8H_{17}), 31.04 (C_{11} , C_8H_{17}), 47.05 (C_{10} , C_8H_{17}), 56.08 (C_{18} , $\text{CH}_2\text{-C}_6\text{H}_4\text{N}_3$), 111.26, 113.99, 114.09, 119.38, 124.86, 126.91, 127.15, 128.54, 130.27, 131.15, 132.41, 143.42 (Ar-C), 145.13 (C_2 , NCHN).

2.3.4 1-Ethyl-3-(1-methylbenzo-1,2,3-triazolyl) benzimidazolium chloride (2d). Yield: 86.31%, white solid, mp 243 °C. FT-IR $\nu(\text{CN})$: 1562 cm^{-1} . ^1H NMR (400 MHz, $\text{DMSO-}d_6$), δ (ppm): 1.55 (t, 3H, H_{11} , C_2H_5), 4.55 (q, 2H, H_{10} , C_2H_5), 7.47 (t, 1H, H_{18} , $\text{C}_6\text{H}_4\text{N}_3$), 7.69 (s, 2H, $\text{H}_{5,6}$, C_6H_4), 7.75 (d, 1H, H_{17} , $\text{C}_6\text{H}_4\text{N}_3$), 7.79 (s, 2H, H_{12} , $\text{CH}_2\text{-C}_6\text{H}_4\text{N}_3$), 8.09 (d, 2H, $\text{H}_{4,7}$, C_6H_4), 8.32 (d, 1H, H_{19} , $\text{C}_6\text{H}_4\text{N}_3$), 8.57 (d, 1H, H_{16} , $\text{C}_6\text{H}_4\text{N}_3$), 10.91 (s, 1H, NCHN). ^{13}C NMR (100 MHz, $\text{DMSO-}d_6$), δ (ppm): 13.89 (C_{11} , C_2H_5), 42.52 (C_{10} , C_2H_5), 56.00 (C_{12} , $\text{CH}_2\text{-C}_6\text{H}_4\text{N}_3$), 111.29, 113.97, 114.06, 119.42, 124.92, 126.89, 127.18, 128.63, 130.40, 131.08, 132.52, 143.17 (Ar-C), 145.12 (C_2 , NCHN).

2.3.5 1-(2-Ethoxyethyl)-3-(1-methylbenzo-1,2,3-triazolyl) benzimidazolium chloride (2e). Yield: 82.35%, white solid, mp: 224.6 °C. FT-IR $\nu(\text{CN})$: 1556.62 cm^{-1} . ^1H NMR (400 MHz,

$\text{DMSO-}d_6$), δ (ppm): 0.98 (s, 3H, H_{13} , $\text{CH}_3\text{CH}_2\text{O}$), 3.43 (m, 2H, H_{12} , $\text{CH}_3\text{CH}_2\text{O}$), 3.83 (s, 2H, H_{10} , $\text{NCH}_2\text{CH}_2\text{O}$), 4.77 (s, 2H, H_{11} , $\text{NCH}_2\text{CH}_2\text{O}$), 7.49 (m, 1H, H_7 , C_6H_4), 7.70 (m, 2H, $\text{H}_{5,6}$, C_6H_4), 7.77 (m, 1H, H_4 , C_6H_4), 7.89 (s, 2H, H_{14} , $\text{CH}_2\text{C}_6\text{H}_4\text{N}_3$), 8.13 (dd, 2H, $\text{H}_{19,20}$, $\text{C}_6\text{H}_4\text{N}_3$), 8.32 (d, 1H, H_{21} , $\text{C}_6\text{H}_4\text{N}_3$), 8.55 (s, 1H, H_{18} , $\text{C}_6\text{H}_4\text{N}_3$), 10.79 (s, 1H, NCHN). ^{13}C NMR (100 MHz, $\text{DMSO-}d_6$), δ (ppm): 14.77 (C_{13} , $\text{CH}_3\text{CH}_2\text{O}$), 47.18 (C_{12} , $\text{CH}_3\text{CH}_2\text{O}$), 56.09 (C_{11} , $\text{NCH}_2\text{CH}_2\text{O}$), 65.55 (C_{10} , $\text{NCH}_2\text{CH}_2\text{O}$), 66.51 (C_{14} , $\text{CH}_2\text{C}_6\text{H}_4\text{N}_3$), 111.09, 113.95, 114.35, 119.51, 124.98, 126.98, 127.22, 128.65, 130.05, 131.27, 132.36, 143.65 (Ar-C), 145.17 (C_2 , NCHN).

2.3.6 1-(2,2-Dimethoxyethyl)-3-(1-methylbenzo-1,2,3-triazolyl)benzimidazolium chloride (2f). Yield: 95%, red solid, mp: 123.5 °C. FT-IR $\nu(\text{CN})$: 1557 cm^{-1} . ^1H NMR (400 MHz, CDCl_3), δ (ppm): 3.43 (s, 6H, $\text{H}_{a,b}$, OCH_3), 4.66–4.67 (d, 2H, H_{10} , $\text{CH}_2\text{CH}(\text{OCH}_3)_2$), 4.79–4.81 (t, 1H, H_{11} , $\text{CH}(\text{OCH}_3)_2$), 7.34–7.38 (t, 1H, H_6 , C_6H_4), 7.56–7.57 (d, 1H, H_5 , C_6H_4), 7.59–7.64 (m, 2H, $\text{H}_{4,7}$, C_6H_4), 7.70–7.72 (d, 1H, H_{18} , $\text{C}_6\text{H}_4\text{N}_3$), 7.92 (s, 2H, H_{12} , $\text{CH}_2\text{C}_6\text{H}_4\text{N}_3$), 7.96–7.9 (d, 1H, H_{17} , $\text{C}_6\text{H}_4\text{N}_3$), 8.30–8.33 (d, 1H, H_{19} , $\text{C}_6\text{H}_4\text{N}_3$), 8.81–8.83 (d, 1H, H_{16} , $\text{C}_6\text{H}_4\text{N}_3$), 12.31 (s, 1H, H_2 , NCHN). ^{13}C NMR (100 MHz, CDCl_3), δ (ppm): 49.53 (C_{10} , $\text{CH}_2\text{CH}(\text{OCH}_3)_2$), 56.19 ($\text{C}_{a,b}$, OCH_3), 57.07 (C_{12} , $\text{CH}_2\text{C}_6\text{H}_4\text{N}_3$), 101.78 (C_{11} , $\text{CH}(\text{OCH}_3)_2$), 111.42, 114.07, 114.43, 119.98, 125.26, 127.74, 127.97, 129.64, 130.50, 132.21, 132.61, 144.84 (Ar-C), 146.14 (C_2 , NCHN).

2.4 General procedure for the preparation of the Pd-PEPPSI complexes (3a–f)

Ligand precursors (2a–f) (1 mmol) were combined with PdCl_2 (1 mmol) and K_2CO_3 in pyridine (5 mL) and stirred at 80 °C for 6 h. After completion of the reaction, pyridine was removed under reduced pressure, and the resulting solid was dissolved in CH_2Cl_2 (10 mL). The solution was filtered through a layer of silica gel and Celite to remove any unreacted PdCl_2 . The filtrate was concentrated under vacuum, and the crude product was dried. Purification was achieved by crystallization from a CH_2Cl_2 /hexane mixture, affording the bright yellow Pd-NHC complexes (3a–f) as pure solids. Yields of the isolated complexes were determined and reported, and the purification procedure was applied consistently for all derivatives to ensure reproducibility.

2.4.1 Dichloro[1-cyclopentyl-3-(1-methylbenzo-1,2,3-triazolyl) benzimidazole-2-ylidene] pyridine palladium(II) (3a). Yield: 61.4%, yellow solid, mp: 231.3 °C. FT-IR $\nu(\text{CN})$: 1448.97 cm^{-1} . ^1H NMR (400 MHz, CDCl_3), δ (ppm): 2.32 (m, 2H, H_{13} , C_5H_9), 2.49 (m, 2H, H_{12} , C_5H_9), 2.63 (m, 2H, H_{14} , C_5H_9), 2.86 (m, 2H, H_{11} , C_5H_9), 3.05 (m, 1H, H_{10} , C_5H_9), 7.63 (m, 2H, $\text{H}_{5,6}$, C_6H_4), 7.83 (m, 1H, H_{18} , $\text{C}_6\text{H}_4\text{N}_3$), 7.96 (m, 2H, $\text{H}_{4,7}$, C_6H_4), 8.06 (m, 2H, $\text{H}_{23,25}$, $\text{C}_5\text{H}_5\text{N}$), 8.34 (s, 2H, H_{15} , $\text{CH}_2\text{C}_6\text{H}_4\text{N}_3$), 8.43 (d, 1H, H_{17} , $\text{C}_6\text{H}_4\text{N}_3$), 8.64 (m, 2H, $\text{H}_{16,24}$, $\text{C}_6\text{H}_4\text{N}_3$, $\text{C}_5\text{H}_5\text{N}$), 9.33 (d, 1H, H_{19} , $\text{C}_6\text{H}_4\text{N}_3$), 9.69 (d, 2H, $\text{H}_{22,26}$, $\text{C}_5\text{H}_5\text{N}$). ^{13}C NMR (100 MHz, CDCl_3), δ (ppm): 25.31 (C_{13} , C_5H_9), 30.18 (C_{12} , C_5H_9), 52.27 (C_{14} , C_5H_9), 53.96 (C_{11} , C_5H_9), 60.30 (C_{11} , C_5H_9), 63.72 (C_{15} , $\text{CH}_2\text{-C}_6\text{H}_4\text{N}_3$), 109.44, 110.71, 111.82, 112.42, 119.98, 121.78, 122.38, 123.82, 124.23, 124.82, 128.57, 132.31, 132.76, 135.03, 138.59, 146.45, 151.45 (Ar-C), 164.81 (C_2 , NCHN).



Elemental analysis (%): calcd. for $C_{24}H_{24}N_6PdCl_2$: C: 50.24; H: 4.22; N: 14.65; found C: 50.2; H: 4.1; N: 14.6.

2.4.2 Dichloro[1-(4-fluorobenzyl)-3-(1-methylbenzo-1,2,3-triazolyl)-5,6-dimethyl benzimidazole-2-ylidene] pyridine palladium(II) (3b). Yield: 75.61%, yellow solid, mp: 147.8 °C; FT-IR $\nu(CN)$: 1509.93 cm^{-1} . 1H NMR (400 MHz, $CDCl_3$), δ (ppm): 2.17 (s, 3H, H_b , $(CH_3)_2C_6H_2$), 2.25 (s, 3H, H_a , $(CH_3)_2C_6H_2$), 6.61 (s, 2H, H_{10} , $CH_2C_6H_4F$), 6.69 (s, 2H, H_{17} , $CH_2-C_6H_4N_3$), 6.94–6.99 (m, 2H, $H_{25,27}$, C_5H_5N), 7.22–7.24 (m, 2H, $H_{12,16}$, C_6H_4F), 7.25–7.26 (m, 2H, $H_{13,15}$, C_6H_4F), 7.29 (s, 2H, $H_{4,7}$, $(CH_3)_2C_6H_2$), 7.37 (t, 2H, $H_{19,20}$, $C_6H_4N_3$), 7.51 (m, 2H, $H_{18,21}$, $C_6H_4N_3$), 8.02 (d, 1H, H_{26} , C_5H_5N), 8.06 (d, 2H, $H_{24,28}$, C_5H_5N). ^{13}C NMR (100 MHz, $CDCl_3$), δ (ppm): 20.10 ($C_{a,b}$, $(CH_3)_2C_6H_2$), 44.40 (C_{10} , $CH_2C_6H_4F$), 52.53 (C_{17} , $CH_2-C_6H_4N_3$), 109.67, 110.53, 110.65, 115.75, 115.96, 119.97, 124.64, 125.85, 127.12, 128.34, 129.07, 129.15, 130.93, 131.25, 131.86, 132.41, 146.35 (Ar-C), 151.44 ($C_{14}-F$), 153.98 (C_2 , NCHN). Elemental analysis (%): calcd. for $C_{28}H_{25}N_6FPdCl_2$: C: 52.39; H: 3.93; N: 13.09; found C: 52.3; H: 4.1; N: 13.1.

2.4.3 Dichloro[1-octyl-3-(1-methylbenzo-1,2,3-triazolyl) benzimidazole-2-ylidene] pyridine palladium(II) (3c). Yield: 63%, yellow solid, mp: 188.9 °C. FT-IR $\nu(CN)$: 1493.99 cm^{-1} . 1H NMR (400 MHz, $CDCl_3$), δ (ppm): 1.27 (s, 3H, H_{17} , C_8H_{17}), 1.53 (s, 2H, $H_{14,15}$, C_8H_{17}), 1.68 (s, 4H, $H_{12,13}$, C_8H_{17}), 2.31–2.33 (m, 8H, $H_{10,11,12,13}$, C_8H_{17}), 4.85–5.00 (m, 2H, H_{18} , $CH_2-C_6H_4N_3$), 6.66–6.76 (m, 1H, H_{20} , $C_6H_4N_3$), 7.12–7.17 (d, 2H, H_{21} , $C_6H_4N_3$), 7.43–7.45 (m, 2H, $H_{26,28}$, C_5H_5N), 7.57 (s, 2H, $H_{4,7}$, $(CH_3)_2C_6H_2$), 7.71 (s, 1H, H_{27} , C_5H_5N), 8.84–7.87 (d, 1H, H_{19} , $C_6H_4N_3$), 8.01–8.06 (d, 1H, H_{22} , $C_6H_4N_3$), 8.64–8.70 (m, 1H, H_{29} , C_5H_5N), 9.09 (s, 1H, H_{25} , C_5H_5N). ^{13}C NMR (100 MHz, $CDCl_3$), δ (ppm): 20.44 (C_{17} , C_8H_{17}), 22.75 (C_{16} , C_8H_{17}), 27.13 (C_{15} , C_8H_{17}), 29.30 (C_{14} , C_8H_{17}), 29.73 (C_{13} , C_8H_{17}), 31.95 (C_{12} , C_8H_{17}), 48.90 (C_{11} , C_8H_{17}), 60.56 (C_{10} , C_8H_{17}), 111.02 (C_{18} , $CH_2-C_6H_4N_3$), 111.29, 119.94, 124.86, 128.55, 133.30, 138.52, 144.23, 144.25, 146.94, 151.45, 162.49 (C_2). Elemental analysis (%): calcd. for $C_{27}H_{32}N_3PdCl_2$: C: 56.31; H: 5.60; N: 7.30; found C: 56.3; H: 5.5; N: 7.3.

2.4.4 Dichloro[1-ethyl-3-(1-methylbenzo-1,2,3-triazolyl) benzimidazole-2-ylidene] pyridine palladium(II) (3d). Yield: 73%, yellow solid, mp: 177.5 °C. FT-IR $\nu(CN)$: 1494.68 cm^{-1} . 1H NMR (400 MHz, $CDCl_3$), δ (ppm): 1.33 (t, 3H, H_{11} , C_2H_5), 3.94 (q, 2H, H_{10} , C_2H_5), 6.69 (s, 2H, H_{12} , $CH_2-C_6H_4N_3$), 7.10 (m, 2H, $H_{5,6}$, C_6H_4), 7.34 (m, 2H, $H_{4,7}$, C_6H_4), 7.52 (m, 2H, $H_{20,22}$, C_5H_5N), 7.76 (m, 2H, $H_{14,15}$, $C_6H_4N_3$), 8.00 (d, 1H, H_{21} , C_5H_5N), 8.06 (d, 2H, $H_{13,16}$, $C_6H_4N_3$), 8.83 (d, 2H, $H_{19,23}$, C_5H_5N). ^{13}C NMR (100 MHz, $CDCl_3$), δ (ppm): 13.59 (C_{11} , C_2H_5), 36.29 (C_{10} , C_2H_5), 52.27 (C_{12} , $CH_2-C_6H_4N_3$), 107.99, 109.42, 110.66, 119.91, 122.06, 122.71, 124.60, 125.08, 127.84, 128.36, 129.06, 132.46, 138.70, 146.28, 151.42 (Ar-C), 153.47 (C_2 , NCHN). Elemental analysis (%): calcd. for $C_{21}H_{21}N_6PdCl_2$: C: 47.17; H: 3.96; N: 15.72; found C: 47.1; H: 3.9; N: 15.7.

2.4.5 Dichloro[1-(2-ethoxyethyl)-3-(1-methylbenzo-1,2,3-triazolyl)benzimidazole-2-ylidene] pyridine palladium(II) (3e). Yield: 59.40%, yellow solid, mp: 212.1 °C. FT-IR $\nu(CN)$: 1495.35 cm^{-1} . 1H NMR (400 MHz, $CDCl_3$), δ (ppm): 1.08 (t, 3H, H_{13} , CH_3CH_2O), 3.44 (q, 2H, H_{12} , CH_3CH_2O), 3.69 (t, 2H, H_{10} , NCH_2CH_2O), 4.06 (t, 2H, H_{11} , NCH_2CH_2O), 6.69 (s, 2H, H_{14} , $CH_2C_6H_4N_3$), 7.08 (m, 2H, $H_{5,6}$, C_6H_4), 7.09 (m, 2H, $H_{4,7}$, C_6H_4),

7.36 (t, 2H, $H_{22,24}$, C_5H_5N), 7.50 (d, 2H, $H_{16,17}$, $C_6H_4N_3$), 7.52 (d, 1H, H_{23} , C_5H_5N), 8.01 (d, 2H, $H_{15,18}$, $C_6H_4N_3$), 8.06 (d, 2H, $H_{21,25}$, C_5H_5N). ^{13}C NMR (100 MHz, $CDCl_3$), δ (ppm): 15.47 (C_{13} , CH_3CH_2O), 42.06 (C_{12} , CH_3CH_2O), 52.63 (C_{10} , NCH_2CH_2O), 67.00 (C_{11} , NCH_2CH_2O), 68.55 (C_{14} , $CH_2C_6H_4N_3$), 109.34, 111.00, 120.23, 122.45, 123.00, 124.91, 128.01, 128.65, 130.14, 132.78, 146.61 (Ar-C), 154.13 (C_2 , NCHN). Elemental analysis (%): calcd. for $C_{23}H_{25}N_6OPdCl_2$: C: 47.73; H: 4.35; N: 14.52; found C: 47.7; H: 4.3; N: 14.5.

2.4.6 Dichloro[1-(2,2-dimethoxyethyl)-3-(1-methylbenzo-1,2,3-triazolyl)benzimidazole-2-ylidene] pyridine palladium(II) (3f). Yield: 54%, yellow crystals, mp: 275.4 °C. FT-IR $\nu(CN)$: 1494.13 cm^{-1} . 1H NMR (400 MHz, $CDCl_3$), δ (ppm): 3.11 (s, 3H, H_{13} , OCH_3), 3.39 (s, 3H, H_{12} , OCH_3), 3.48–3.50 (d, 2H, H_{10} , $CH_2CH(OCH_3)_2$), 5.11–5.29 (m, 1H, H_{11} , $CH(OCH_3)_2$), 6.70 (s, 1H, H_{23} , C_5H_5N), 7.09 (s, 2H, H_{14} , $CH_2C_6H_4N_3$), 7.21–7.27 (m, 2H, $H_{5,6}$, C_6H_4), 7.39 (m, 2H, $H_{16,17}$, $C_6H_4N_3$), 7.53 (d, 2H, $H_{4,7}$, C_6H_4), 7.78 (m, 2H, $H_{22,24}$, C_5H_5N), 7.87–8.07 (m, 2H, $H_{15,18}$, $C_6H_4N_3$), 8.69 (s, 1H, H_{25} , C_5H_5N), 9.08 (s, 1H, H_{21} , C_5H_5N). ^{13}C NMR (100 MHz, $CDCl_3$), δ (ppm): 54.67 (C_{13} , OCH_3), 54.90 (C_{12} , OCH_3), 56.08 (C_{10} , $CH_2CH(OCH_3)_2$), 61.25 (C_{14} , $CH_2C_6H_4N_3$), 102.10 (C_{11} , $CH(OCH_3)_2$), 102.99, 104.17, 104.76, 108.97, 109.19, 110.52, 111.64, 111.74, 112.02, 119.85, 122.19, 122.73, 124.36, 124.90, 128.24, 128.63, 146.60 (Ar-C), 151.25 (C_2 , NCHN). Elemental analysis (%): calcd. for $C_{23}H_{24}N_6PdCl_2$: C: 49.17; H: 4.31; N: 14.96; found C: 49.1; H: 4.3; N: 14.8.

2.5 General procedure for the *N*-alkylation of aniline with alcohols

Under the optimized conditions, a mixture of an aniline derivative (1.0 mmol), an excess of the alcohol derivative (1.5 mmol), $KOtBu$ (1.0 mmol), and the Pd-PEPPSI catalyst (**3a-f**) (2.5 mol%) was placed in a J. Young tube and stirred at 150 °C for 24 h under an argon atmosphere. After cooling to room temperature, CH_2Cl_2 (2 mL) was added to the reaction mixture. The resulting solution was filtered through a short silica gel pad, and the filtrate was analyzed by GC-MS.

2.6 Antimicrobial methods and anticancer (MTT) tests

The MTT tests were performed according to our previous work.^{39,40}

3 Results and discussion

3.1 Synthesis of benzimidazolium salts 2a-f

The target benzimidazolium salts **2a-f** were synthesized through a two-step *N*-alkylation strategy, as outlined in Scheme 1. In the first step, selective *N*-alkylation of benzimidazole or 5,6-dimethylbenzimidazole (**1**) was performed to introduce an alkyl substituent, thereby enhancing the nucleophilicity of the remaining nitrogen atom. This initial alkylation was achieved using six different alkylating agents, 4-fluorobenzyl chloride, cyclopentyl chloride, octyl chloride, ethyl chloride, 2-chloroethoxyethane, and 2-chloro-1,1-dimethoxyethane, in DMSO under reflux conditions for 24 h. The resulting mono-*N*-alkylated benzimidazolium salts (**1a-f**) were isolated by



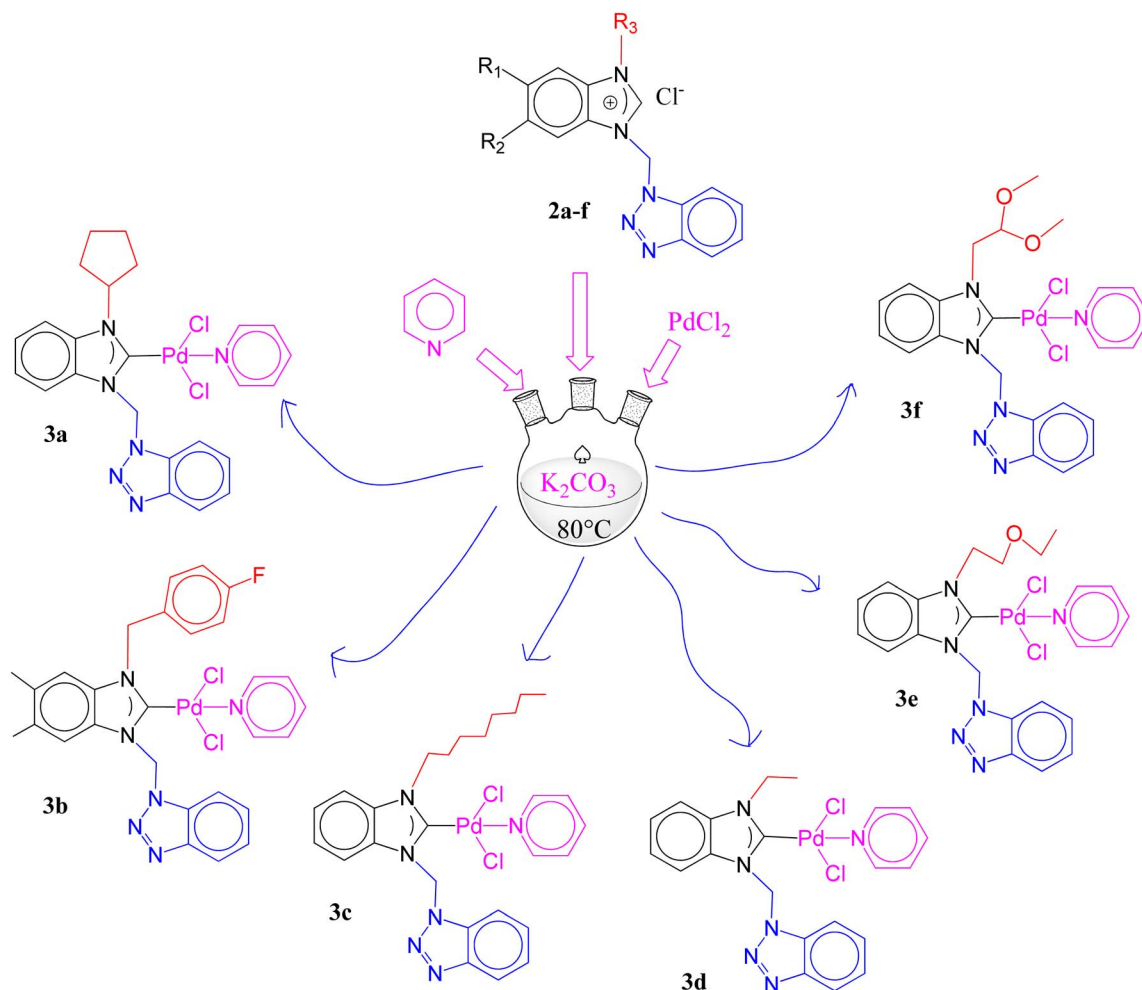
Table 1 Physical data and yields of the benzimidazolium chlorides 2a–f

Code	Chemical formula	Melting point (°C)	Physical appearance	Yield (%)	$\nu_{(\text{CN})}$	^1H (NCHC)	^{13}C (NCHC)
2a	$\text{C}_{19}\text{H}_{21}\text{N}_5\text{Cl}$	234	Brown solid	100	1563	12.52	145.91
2b	$\text{C}_{23}\text{H}_{22}\text{N}_5\text{ClF}$	235.4	White solid	70.61	1554	12.54	146.01
2c	$\text{C}_{22}\text{H}_{29}\text{N}_5\text{Cl}$	131.5	Purple solid	67.98	1560.03	11.11	145.13
2d	$\text{C}_{16}\text{H}_{17}\text{N}_5\text{Cl}$	243	White solid	86.31	1562	10.91	145.12
2e	$\text{C}_{18}\text{H}_{21}\text{N}_5\text{OCl}$	220.3	White solid	82.35	1552.62	10.79	145.17
2f	$\text{C}_{18}\text{H}_{21}\text{N}_5\text{O}_2\text{Cl}$	123.5	Red solid	95	1557	12.31	146.14

precipitation with diethyl ether and obtained in good to excellent yields (77–90%). In the second step, *N,N*-disubstituted benzimidazolium salts 2a–f were obtained by subsequent alkylation of the remaining nitrogen atom with chloromethylbenzotriazole in DMF at 80 °C for 24 h. The resulting salts exhibited good solubility in polar solvents such as methanol, ethanol, DMSO, and DMF, while remaining insoluble in non-polar solvents, including diethyl ether, dichloromethane, and chloroform. All benzimidazolium salts 2a–f were found to be stable toward air and moisture, both in the solid state and in solution. Structural characterization of the synthesized salts was accomplished using FT-IR spectroscopy, ^1H and ^{13}C NMR

spectroscopy, elemental analysis, and X-ray diffraction techniques. Selected physical and spectroscopic data of the novel compounds are summarized in Table 1.

The synthesized compounds 2a–f were thoroughly characterized using FT-IR, ^1H , ^{13}C , and ^{19}F NMR spectroscopy, as well as elemental analysis (see Experimental Section and SI). In the ^1H NMR spectra, the acidic C(2)–H proton of 2a–f appeared as sharp singlets at $\delta = 13.31, 12.52, 12.54, 11.11, 10.91,$ and 10.79 – 10.01 ppm, respectively, confirming protonation at the C(2) position. The corresponding ^{13}C NMR spectra displayed the C(2) carbon resonances at $\delta = 145.9, 146.0, 145.1, 145.12, 145.17,$ and 146.14 ppm, consistent with formation of the



Scheme 2 Synthesis of palladium(II)–PEPSI complexes 3a–f.



desired salts. FT-IR analysis further supported the structures, revealing characteristic $\nu(\text{C}=\text{N})$ stretching bands at 1563, 1554, 1560, 1562, 1556, and 1557 cm^{-1} for **2a-f**, in agreement with previously reported values.⁴¹ The aromatic protons (Ar-H) appeared as multiplets in the ranges δ 7.28–7.89 ppm and δ 7.10–7.79 ppm, corresponding to the substituted and unsubstituted arene moieties, respectively. Collectively, these spectroscopic data confirm the successful synthesis and structural integrity of the NHC salts **2a-f**.

3.2 Synthesis and characterization of Pd-PEPPSI complexes containing triazole ligands

Six novel benzimidazole-based Pd-PEPPSI complexes (**3a-f**) incorporating triazole-functionalized NHC ligands were successfully synthesized *via* the reaction of the corresponding benzimidazolium salts **2a-f** with PdCl_2 and pyridine in the presence of K_2CO_3 , as illustrated in Scheme 2. The reactions proceeded smoothly under mild conditions and were completed within 6 h, affording the desired complexes in good yields. The incorporation of the triazole moiety into the NHC framework proved to be an efficient strategy for stabilizing the Pd(II)-PEPPSI architecture. All resulting palladium complexes exhibited excellent stability toward air, moisture, and light, both in solution and in the solid state, and could be stored at room temperature for extended periods without any observable degradation or loss of catalytic performance. Furthermore, the complexes showed good solubility in common organic solvents, such as dichloromethane, chloroform, ethyl acetate, and DMSO, while remaining insoluble in non-polar solvents, including pentane and hexane. Overall, this straightforward synthetic approach provides reliable access to robust Pd-PEPPSI complexes bearing triazole-functionalized NHC ligands, highlighting their suitability as stable and versatile precatalysts for catalytic applications.

The complexes were characterized by ^1H and ^{13}C NMR and FT-IR spectroscopy. In the ^1H NMR spectra, the disappearance of the acidic C(2)-H signal of the parent salts **2a-f** confirms the formation of the carbene ligand. Downfield resonances at δ = 6.70–9.69 ppm correspond to the aromatic protons of the pyridine ring, indicating its coordination to the palladium center and the formation of PEPPSI-type complexes. The ^{13}C NMR spectra revealed the corresponding C(2) carbon resonances between δ = 145.12 and 146.14 ppm. These downfield signals are consistent with the formation of salts **2a-f**. While the characteristic Pd-C(2) carbene signals of complexes **3a-f** appear as singlets at δ = 164.81, 153.98, 162.49, 153.47, 154.13 and 151.25 ppm, respectively, further supporting complex formation. FT-IR analysis shows characteristic $\nu(\text{C}=\text{N})$ stretching bands at 1448.97, 1509.93, 1493.99, 1494.68, 1495.35 and 1494.13 cm^{-1} for complexes **3a-f**, respectively. The peak shift to lower frequency is attributed to electron donation from the carbene ligand to the palladium center, which weakened the C=N bond Fig. 1. Overall, the spectroscopic features of these complexes are consistent with previously reported Pd-PEPPSI systems.⁴²

Aromatic protons from the benzimidazole and benzotriazole rings appear as multiplets at δ 7.63–9.33 ppm, consistent with the presence of the heteroaromatic framework. The CH_2 group connecting the benzotriazole and benzimidazole typically appears as a singlet around δ 8.34 ppm, confirming the successful coordination without disruption of the *N*-alkyl linkage. Signals corresponding to *N*-cyclopentyl substituents appear as multiplets at δ 2.32 and 3.05 ppm, depending on the chain length and branching (Fig. 2).

The NCN carbon of the benzimidazole precursor appears at 164.81 ppm, shifted slightly downfield compared to the free ligands due to coordination with Pd(II). The quaternary carbon

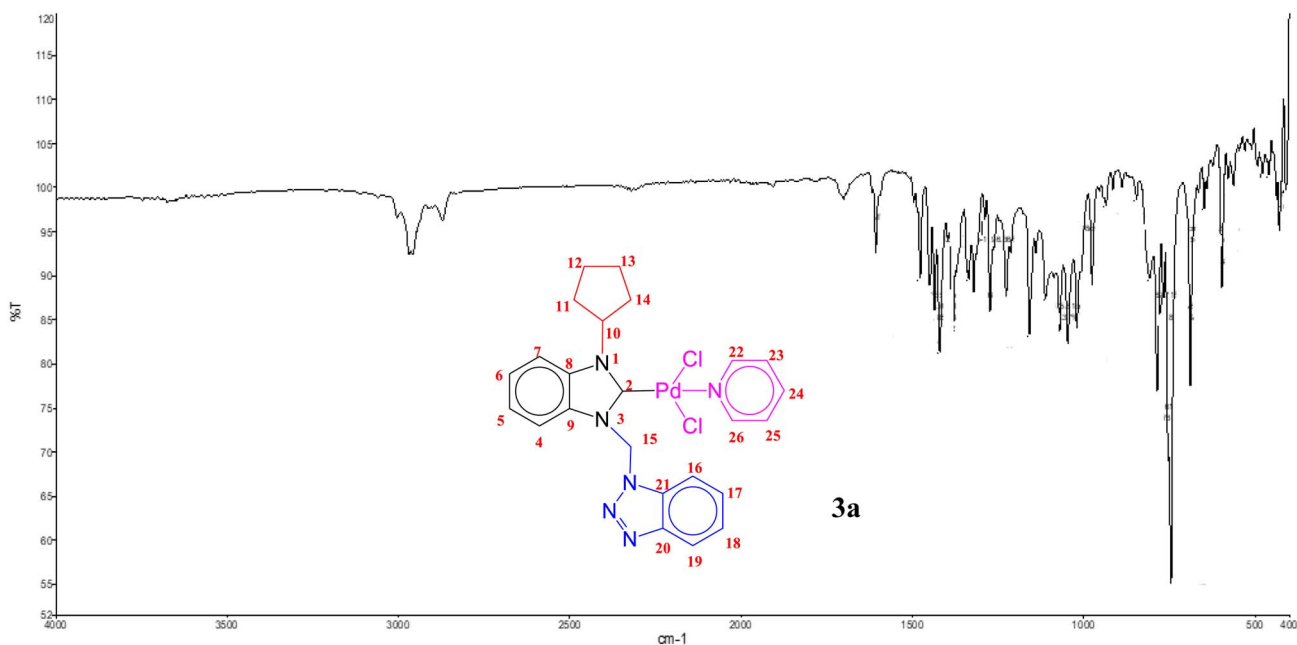


Fig. 1 IR spectrum of complex **3a**.

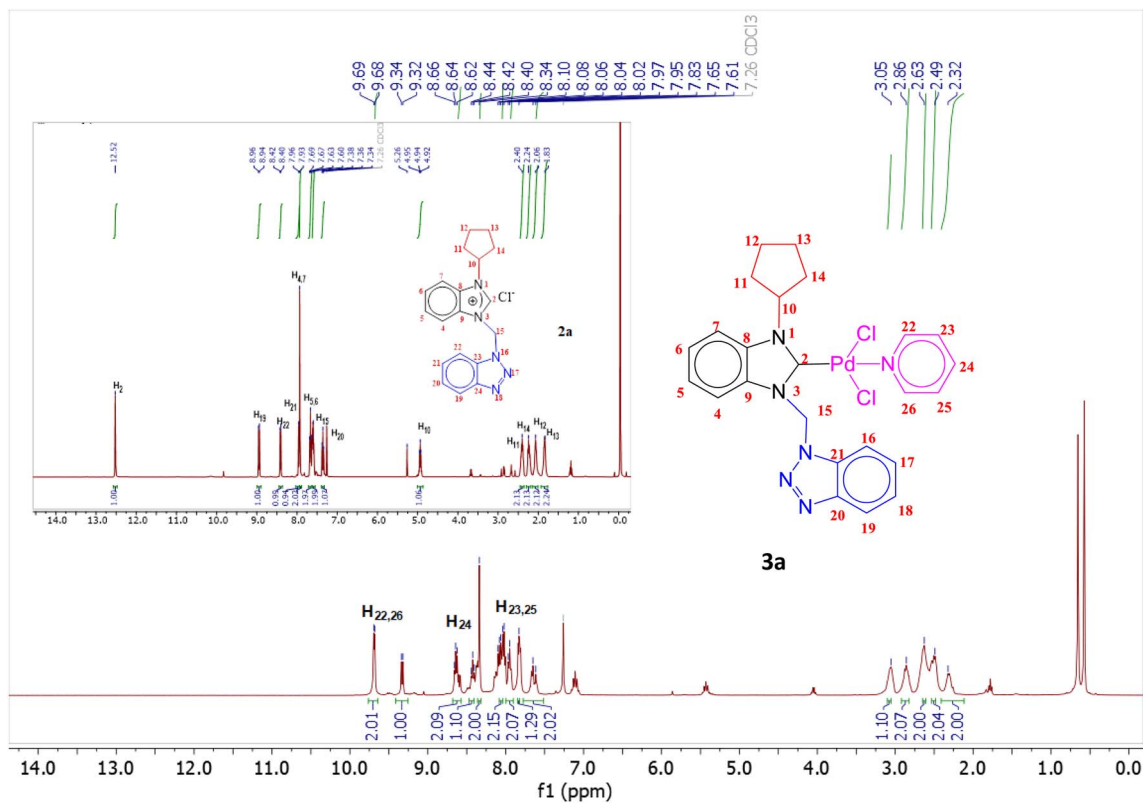
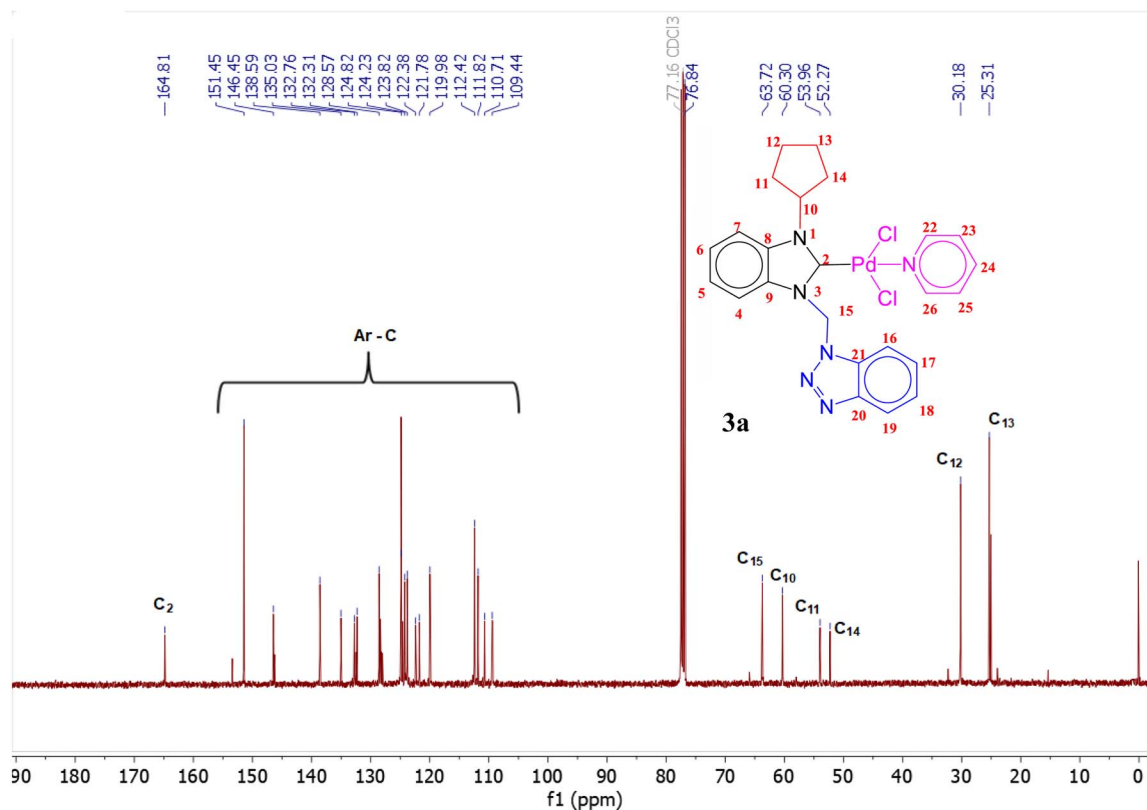
Fig. 2 ^1H NMR spectra of complex 3a.Fig. 3 ^{13}C NMR spectrum of complex 3a.

Table 2 Physical data and yields for Pd–PEPPSI complexes 3a–f

Code	Chemical formula	Melting point (°C)	Physical appearance	Yield (%)	ν_{CN}	^{13}C (NCHC)	^1H (pyridine)
3a	C ₂₄ H ₂₄ N ₆ PdCl ₂	231.3	Yellow solid	61.4	1448.97	164.81	8.06–9.69
3b	C ₂₈ H ₂₅ N ₆ FPdCl ₂	147.8	Yellow solid	75.61	1509.93	153.98	6.94–8.06
3c	C ₂₇ H ₃₂ N ₃ PdCl ₂	189.1	Yellow solid	63.0	1493.99	162.49	7.43–9.09
3d	C ₂₁ H ₂₁ N ₆ PdCl ₂	177.5	Yellow solid	73.0	1494.68	153.47	7.52–8.83
3e	C ₂₃ H ₂₅ N ₆ OPdCl ₂	212.1	Yellow solid	59.40	1495.35	154.13	7.36–8.06
3f	C ₂₃ H ₂₄ N ₆ O ₂ PdCl ₂	275.4	Yellow crystals	54.0	1494.13	151.25	7.78–9.08

attached to nitrogen shows a signal at δ 60.30 ppm, confirming *N*-alkylation and metal coordination. The CH₂ carbon connecting benzimidazole and benzotriazole shifts slightly downfield to δ 60.72 ppm upon coordination, consistent with electron withdrawal by Pd(II) (Fig. 3).

Overall, the NMR spectra demonstrate complete coordination of the NHC ligands to Pd(II), while retaining the integrity of the benzimidazole framework. The downfield shifts of the protons and carbons adjacent to the coordinating nitrogen atoms provide strong evidence for metal–ligand bonding.

The C=N stretching vibration of the benzimidazole rings is observed at 1448.97 cm⁻¹. C–H stretching vibrations of *N*-alkyl and benzotriazole substituents are observed at 2969.70 cm⁻¹. Bands between 1158.65 and 1226.30 cm⁻¹ correspond to C–N stretching of the coordinated heterocyclic nitrogen, shifted compared to that of the free ligand, consistent with Pd–N coordination. Aromatic bending vibrations appear around 648.14–934.98 cm⁻¹, confirming retention of the aromatic rings after complexation. The absence of N–H stretching (normally ~3200–3400 cm⁻¹ in the free ligands) confirms full *N*-alkylation and coordination, leaving no free NH protons (Fig. 1).

The NMR and elemental analysis results showed that all the complexes obtained have NHC and pyridine ligand in 1 : 1 stoichiometry. The melting points of the compounds ranged from 110 to 300 °C. The selected physical and spectroscopic data of the novel compounds are summarized in Table 2.

3.3 X-ray crystallography

Single-crystal diffraction data were collected at 100(2) K with a Bruker D8 Venture diffractometer using graphite-monochromated MoK α at a wavelength of 0.71073 Å. The structure was solved by the SHELXT-2018/2 method⁴³ in the monoclinic space group *P*2₁/*n* and refined by the full-matrix least squares technique on F^2 with SHELXL-2019/1.⁴⁴ All H atoms were located in difference maps and then treated as riding atoms, fixing the bond lengths at 0.95, 0.99 and 0.98 Å for aromatic CH, CH₂ and CH₃ atoms, respectively. The displacement parameters of the H atoms were fixed at $U_{\text{iso}}(\text{H}) = 1.2U_{\text{eq}}$ (1.5 U_{eq} for CH₃).

CCDC: 2521078 contains the supplementary crystallographic data for compound 3f, reported in this article.

3.3.1 Theoretical methods. The geometry optimization of the structure was carried out from the structure obtained by single-crystal determination. The structure was optimized with the DFT method and the Gaussian 09 program.⁴⁵ The

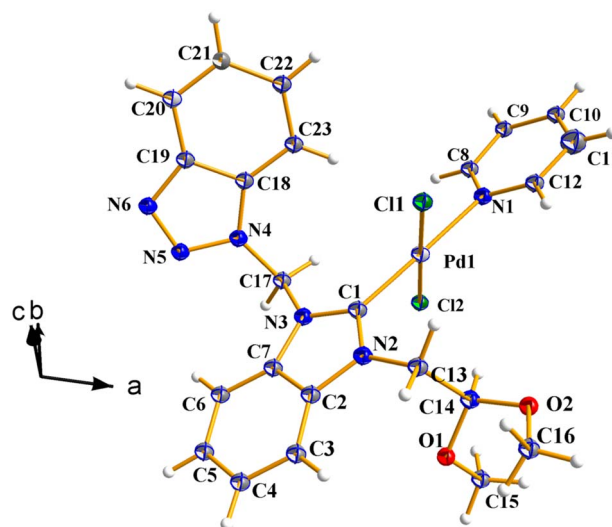


Fig. 4 View of the crystal structure of the title compound 3f (thermal ellipsoids shown at the 50% probability level).

calculations were performed using the B3LYP, CAM-B3LYP and M06-2X functional. The Hirshfeld surfaces and the associated 2D fingerprint plot were calculated using Crystal Explorer 3.1.⁴⁶

3.3.2 Crystal structure. The molecular structure of the palladium organometallic complex 3f with the adopted atom-labelling scheme is shown in Fig. 4, and important bond distances are listed in Table S1. The palladium complex crystallized in the monoclinic space group *P*2₁/*n* (Table S1). The

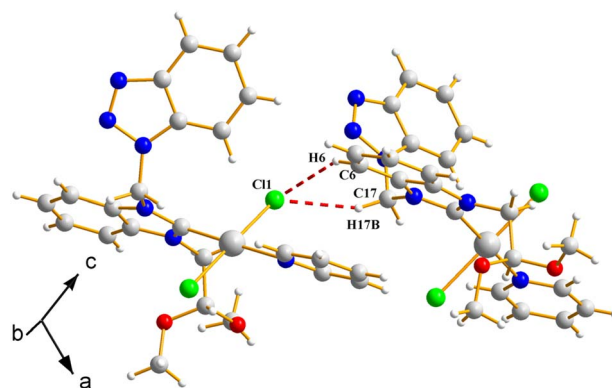


Fig. 5 Crystal structure of the title organometallic complex 3f, showing the intermolecular hydrogen bonds C–H...Cl (dashed red lines).



Table 3 Selected hydrogen bonds for C₂₃H₂₄Cl₂N₆O₂Pd (3f)^a

D-H...A	D-H (Å)	H...A (Å)	D...A (Å)	<(DHA)> (°)
C13)-H13B...Cl1	0.99	2.65	3.4574(14)	139.2
C15)-H15A...Cl2 ⁱ	0.98	2.77	3.7408(17)	173.0
C6-H6...Cl1 ⁱⁱ	0.95	2.78	3.6204(14)	147.9
C17-H17A...Cl2	0.99	2.75	3.4215(13)	125.9
C17-H17B...Cl1 ⁱⁱ	0.99	2.64	3.5698(13)	156.8

^a Symmetry codes: (i) $-x + 3/2, y - 1/2, -z + 1/2$; (ii) $x - 1/2, -y + 3/2, z - 1/2$.

complex shows a slightly distorted square-planar coordination geometry around the Pd(II) center, where the Pd(II) ions are four-coordinated with one carbene ligand, two chloride ligands and one NHC (*N*-heterocyclic carbene) ligand. In this coordination geometry, the Pd-C1 (1.9645(12) Å) and Pd-N1 (2.0868(11) Å) bond lengths are relatively short, while Pd-Cl1 and Pd-Cl2 are elongated to 2.2817(3) Å and 2.2997(4) Å, respectively. Bond distances between the Pd1 center and the atoms of the ligands are in perfect agreement with those observed in other very similar complexes.⁴⁷⁻⁴⁹

The palladium complex was held together by extended intra- and intermolecular C-H...Cl hydrogen bonds (Fig. 5 and Table 3) with strong contributions from the carbene ligand and the

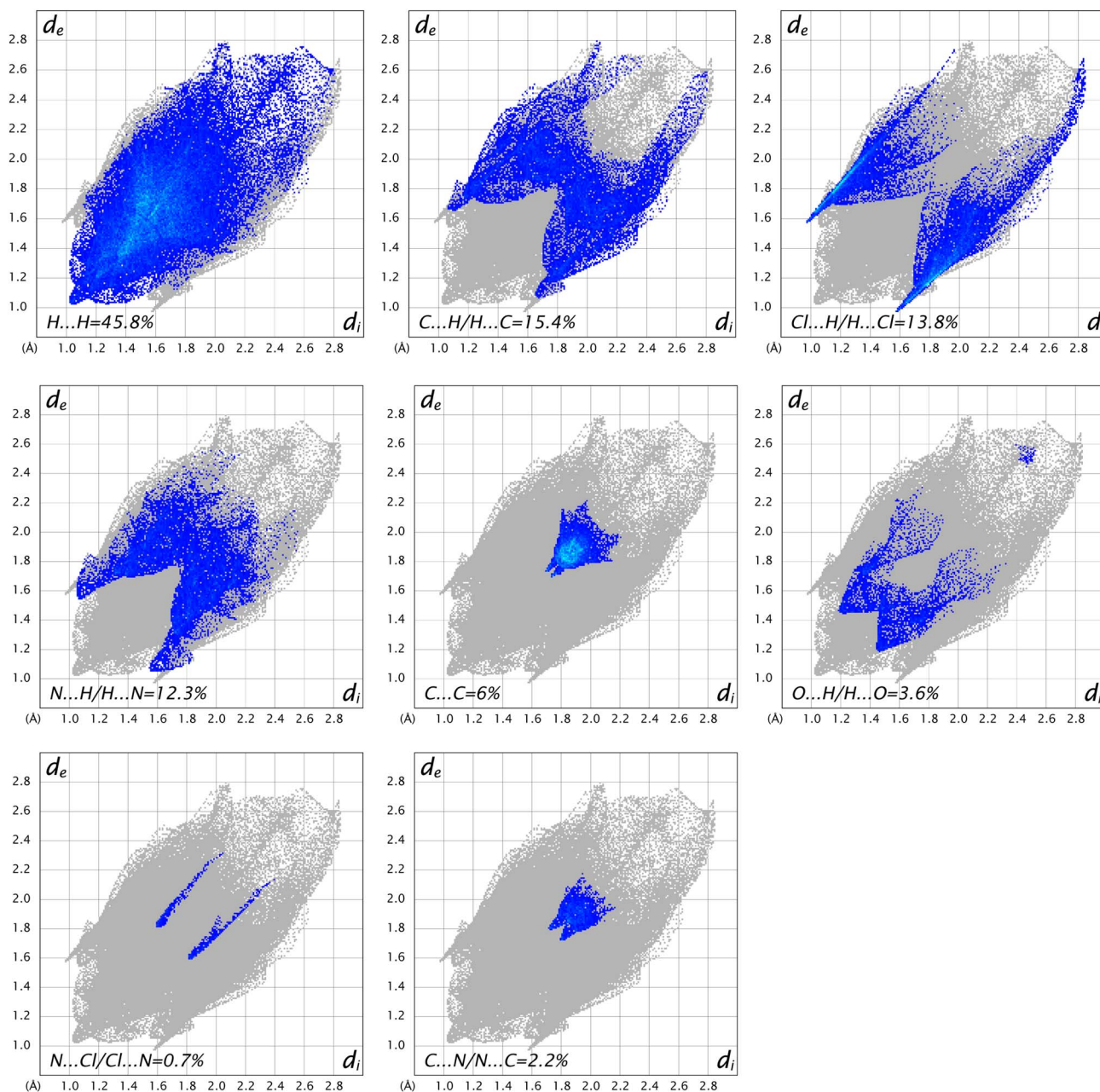


Fig. 6 2D fingerprint plots of the title compound 3f.



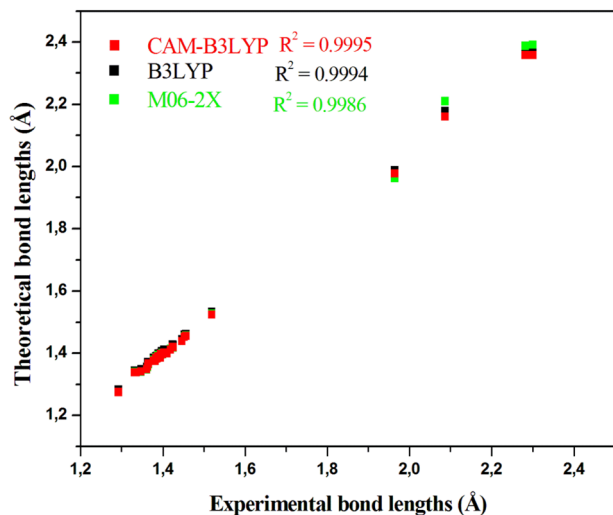


Fig. 7 Graphical correlation between experimental and calculated bond lengths and angles obtained with different functionals for the title carbene compound 3f.

two chloride ligands. Overall, the A...H and D...A distances cover a range of 2.64 Å and 3.74 Å, respectively, and thus are assigned as weak hydrogen bonds.^{50–52}

The Hirshfeld surface was calculated and mapped over d_{norm} , confirming the intermolecular interactions in addition to the van der Waals interactions. The 2-D fingerprint plots (Fig. 6) show that the H...H contacts cover 45.8% of the total surface, followed by C...H, Cl...H and N...H contacts with 15.4, 13.8 and 12.3%, respectively. Minor contributions come from C...C (6%), O...H (3.6%), N...Cl (0.7%) and N...C (2.2%) contacts. These results are consistent with multiple C–H...Cl hydrogen bonding interactions.

3.3.3 DFT-calculated optimized geometry. The geometry of the molecular structure of 3f was optimized using the B3LYP, CAM-B3LYP and M06-2X functionals, and all showed good agreement with the data obtained from X-ray diffraction (Table S2). These results were confirmed by the calculated correlation coefficient between experimental and calculated data (Fig. 7).

3.4 Antimicrobial activity

The antimicrobial activities of the benzimidazolium salts (2a–f) and their Pd–PEPPSI complexes (3a–f) were evaluated against *Escherichia coli*, *Pseudomonas aeruginosa*, *Staphylococcus aureus*, *Candida albicans* and *Candida glabrata* strains at different concentrations; Ampicillin and Caspofungin were used as standards. The antibacterial and antifungal activities of the compounds were determined using the disk diffusion test; the inhibition zones of the synthesized compounds are summarized in Table 4.

According to the results, ligand derivatives 2e and 2f showed no antibacterial or antifungal activities against *P. aeruginosa*, *C. albicans* or *C. glabrata* strains. Also, 3a, 3b, 3c, 3d and 3f complexes did not show antifungal activity against *C. albicans* or *C. glabrata* yeast species. Among the 2a, 2b, 2c, and 2d ligands and 3e complex, 2c showed the highest activity against the two fungi strains, with 15.2 ± 0.21 mm and 11.7 ± 0.21 mm, respectively; all compounds had smaller inhibition zones than the reference antibiotic. When the antibacterial activities of the synthesized 1,3-disubstituted benzimidazolium chlorides (2a–f) and the corresponding complexes (3a–f) were examined, the largest inhibition zones against *E. coli* and *S. aureus* were formed for 2c at 15.2 ± 0.25 mm and 23.6 ± 0.69 mm, respectively. It was observed that 2b and 2d had larger inhibition zones, with 20.4 ± 0.66 mm and 22.1 ± 0.15 mm against *S. aureus*, while all the compounds showed less inhibition activity than ampicillin. Complex 3d showed the best activity among the synthesized compounds, with 14.8 ± 1.11 mm against *P. aeruginosa*. Complexes 3c and 3f also had larger zones than the standard drug against *P. aeruginosa*.

The results of the disk diffusion tests revealed that the highest antimicrobial activity was for 1,3-disubstituted benzimidazolium chloride 2c compared to the other compounds, against the tested organisms except for *P. aeruginosa*.

3.5 Anticancer activities

In this study, the anticancer activities of six benzimidazolium ligands (2a–f) and their corresponding Pd–PEPPSI complexes

Table 4 Antifungal and antibacterial inhibition zone values (mm)

Compounds	Antifungal		Antibacterial		
	<i>C. albicans</i>	<i>C. glabrata</i>	<i>E. coli</i>	<i>P. aeruginosa</i>	<i>S. aureus</i>
2a	NIZ	6.4 ± 0.17	8.6 ± 0.21	6.4 ± 0.17	14.9 ± 0.1
2b	11.2 ± 0.17	6.7 ± 0.12	8.6 ± 0.21	7 ± 0.08	20.4 ± 0.66
2c	15.2 ± 0.21	11.7 ± 0.21	15.2 ± 0.25	7.9 ± 0.17	23.6 ± 0.69
2d	12.6 ± 0.29	7.3 ± 0.54	13.5 ± 0.25	7 ± 0.16	22.1 ± 0.15
2e	NIZ	NIZ	8.1 ± 0.29	NIZ	14.3 ± 0.35
2f	NIZ	NIZ	8.6 ± 0.17	NIZ	12.8 ± 0.25
3a	NIZ	NIZ	NIZ	12.4 ± 0.43	7.7 ± 0.25
3b	NIZ	NIZ	7.5 ± 0.37	10.3 ± 0.26	11.6 ± 0.53
3c	NIZ	NIZ	7.2 ± 0.21	13.2 ± 1.31	10.6 ± 0.51
3d	NIZ	NIZ	7.5 ± 0.12	14.8 ± 1.11	8.4 ± 6.28
3e	6.8 ± 0.16	7 ± 0.33	8.1 ± 0.29	7.5 ± 0.41	7.9 ± 0.12
3f	NIZ	NIZ	6.8 ± 0.09	13.6 ± 0.42	8.3 ± 0.25
Ampicillin	—	—	18.2 ± 1.84	12.5 ± 0.41	15.3 ± 0.25
Caspofungin	23.5 ± 0.36	26.5 ± 0.39	—	—	—



Table 5 Anticancer activities and inhibitory concentration values (μM)^a

Entry	Compounds	IC ₅₀ (μM)			SI	
		BEAS2B	HCT116	A549	HCT116	A549
1	2a	9.81 ± 0.89	NA	273.66 ± 14.11	—	0.04
2	2b	137.24 ± 1.34	170.13 ± 75.06	40.84 ± 1.64	8.01	3.36
3	2c	3.92 ± 0.10	0.86 ± 0.06	15.73 ± 3.75	4.56	0.25
4	2d	17.38 ± 1.83	73.04 ± 3.35	43.63 ± 6.53	0.24	0.40
5	2e	NA	NA	221.69 ± 14.68	—	—
6	2f	NA	NA	249.40 ± 9.78	—	—
7	3a	236.6 ± 20.96	151.34 ± 7.99	568.9 ± 24.99	1.56	0.42
8	3b	32.3 ± 1.38	22.57 ± 2.83	88.5 ± 11.63	1.43	0.36
9	3c	265.2 ± 27.19	293.02 ± 30.88	300.2 ± 52.23	0.918	0.88
10	3d	93.4 ± 6.61	69.18 ± 10.49	205.8 ± 25.06	1.35	0.45
11	3e	152.2 ± 4.29	113.15 ± 7.37	75.2 ± 12.73	1.35	2.02
12	3f	120 ± 4.55	161.76 ± 23.05	313.3 ± 3.91	0.74	0.38
CISPLATIN	CONTROL	103.26 ± 3.26	254.78 ± 6.11	189.44 ± 5.13	0.41	0.55

^a IC₅₀ values presented as mean ± SD of three independent experiments. NA: not applicable (IC₅₀ > 800 μM). Cell lines. Reference Drug. SI = IC₅₀ values of BEAS2B/IC₅₀ values of cancer cells.

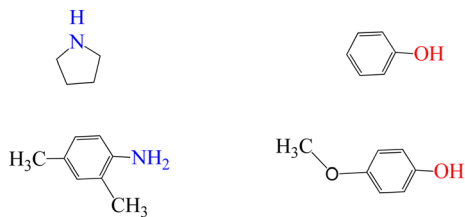
(3a–f) were evaluated using the MTT assay against one healthy cell line, BEAS-2B (human bronchial epithelial cells), and two cancer cell lines, HCT116 (human colorectal carcinoma) and A549 (human lung carcinoma), with cisplatin used as the reference drug. The biological samples used in this study were obtained from İnönü University (Malatya, Turkey). The human bronchial epithelial cell line BEAS-2B, the human colorectal carcinoma cell line HCT116, and the human lung carcinoma cell line A549 were provided by İnönü University. The IC₅₀ values of cisplatin were determined to be 103.26 ± 3.26 μM for BEAS-2B, 254.78 ± 6.11 μM for HCT116, and 189.44 ± 5.13 μM for A549. All cell lines were maintained and handled according to standard cell culture protocols. Authentication and routine mycoplasma testing were performed prior to experimental use. All synthesized compounds exhibited measurable cytotoxicity against the tested cell lines (IC₅₀ < 800 μM) and, in general, showed higher cytotoxic activity than cisplatin under the same experimental conditions. However, a critical examination of the data reveals that cytotoxicity toward the healthy BEAS-2B cell line remains a significant consideration when assessing the therapeutic potential of these compounds. Although several compounds displayed enhanced activity against cancer cells, none of the tested ligands or Pd–PEPPSI complexes were completely non-toxic to BEAS-2B cells, indicating limited absolute selectivity.

Notably, complexes 3a and 3c exhibited the lowest cytotoxicity across all three cell lines, including BEAS-2B, suggesting a more moderate biological profile that may be advantageous for further structural optimization. In contrast, complex 3b showed the highest cytotoxic activity against both cancerous and healthy cells, indicating potent but relatively non-selective behavior. While such strong cytotoxicity may be desirable for anticancer efficacy, the comparable toxicity toward BEAS-2B cells raises concerns regarding potential off-target effects and therapeutic window limitations. When the IC₅₀ values for healthy and cancerous cell lines were compared, all compounds demonstrated higher cytotoxic activity toward the A549 lung

cancer cell line relative to BEAS-2B cells, suggesting a degree of preferential activity toward malignant lung cells. In particular, compounds 2b, 3a, 3c, 3e, and 3f showed reduced cytotoxicity toward BEAS-2B cells compared to their activity against cancer cell lines, indicating an improved but still moderate selectivity profile. Conversely, several compounds displayed lower IC₅₀ values against BEAS-2B cells than against the HCT116 cell line, highlighting a lack of selectivity toward colorectal cancer cells and underscoring the need for caution in interpreting overall anticancer efficacy. Overall, while the Pd–PEPPSI complexes demonstrate promising anticancer activity, their cytotoxic effects on healthy BEAS-2B cells suggest that further ligand modification and structure–activity relationship studies are necessary to enhance cancer cell selectivity and reduce off-target toxicity. Future investigations should include selectivity index calculations, mechanistic studies, and evaluation against additional normal cell lines to better assess their potential as viable anticancer agents.

To better assess the anticancer potential of the synthesized benzimidazolium ligands (2a–f) and their corresponding Pd–PEPPSI complexes (3a–f), cytotoxicity results were interpreted not only on the basis of IC₅₀ values but also using selectivity indices (SI), defined as the ratio of the IC₅₀ value for the healthy cell line (BEAS-2B) to that for the corresponding cancer cell line (Table 5). This parameter provides a more meaningful measure of therapeutic relevance by directly reflecting the preference of a compound for cancerous cells over normal cells. In general, SI values greater than 1 indicate selective cytotoxicity toward cancer cells, whereas SI values close to or below 1 suggest limited or poor selectivity. Using this approach, all the synthesized compounds exhibited SI values greater than unity for the A549 lung cancer cell line, indicating a consistent preference for malignant lung cells over healthy bronchial epithelial cells. This observation suggests that both the benzimidazolium ligands and their Pd–PEPPSI complexes possess an inherent tendency to target lung cancer cells, possibly due to differences in cellular uptake, metabolic activity, or sensitivity to palladium-based



Scheme 3 Amines and alcohols used in the *N*-alkylation reactions.

species. Nevertheless, the magnitude of the SI values varied considerably among the compounds, highlighting the influence of ligand structure on biological selectivity. Complexes **3a** and **3c**, which displayed higher IC_{50} values toward BEAS-2B cells and moderate activity against cancer cells, resulted in improved SI values, indicating a more favorable balance between anticancer efficacy and toxicity toward normal cells. In contrast, complex **3b**, despite exhibiting the highest overall cytotoxicity, showed lower SI values due to its pronounced toxicity toward BEAS-2B cells. This behavior suggests that the high potency of **3b** is accompanied by reduced selectivity, which may limit its therapeutic applicability without further structural refinement.

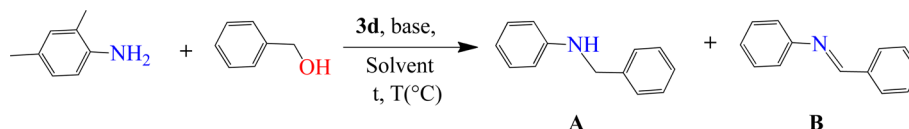
For the HCT116 colorectal cancer cell line, several compounds exhibited SI values close to or below unity, reflecting either comparable or higher toxicity toward BEAS-2B cells than toward cancer cells. This lack of selectivity underscores a key limitation of the current compound set and indicates that the observed cytotoxic effects may arise from general cellular toxicity rather than cancer-specific mechanisms. Consequently, while the Pd-PEPPSI complexes demonstrate promising anticancer activity, their selectivity toward colorectal cancer cells remains insufficient at this stage. Overall, the inclusion of selectivity indices provides a more critical and realistic

evaluation of the biological performance of these compounds. Although enhanced activity against A549 cells is encouraging, the measurable toxicity toward BEAS-2B cells emphasizes the need for further ligand optimization to improve selectivity and widen the therapeutic window. Future work should focus on structure-selectivity relationship studies, mechanistic investigations, and evaluation across a broader panel of normal cell lines to better define the anticancer potential of Pd-PEPPSI-NHC systems. The SI calculations showed that compound **2b** was the most promising among all evaluated compounds, showing SI values of 8 and 4.56 against the two cancer cell lines. Compound **2c** ranked second in terms of activity.

3.6 Catalytic activity of the complexes

The synthesized Pd-PEPPSI complexes (**3a-f**) were evaluated as catalysts for the *N*-alkylation of representative amines with alcohol derivatives (Scheme 3). In this transformation, two products may form: the *N*-alkylated amine (A) or the corresponding imine intermediate (B). Optimization studies were conducted using aniline and benzyl alcohol as a model reaction with complex **3d**; the results are summarized in the optimization table shown in Table 6.

Control experiments confirmed the necessity of both the palladium catalyst and the base, as reactions performed in the absence of either component showed negligible conversion (Table 6, entries 1 and 10). The effect of the catalyst loading was also examined, and reproducibility tests demonstrated that reduced palladium loadings remain effective and reliable. Screening of various bases, including KOH, K_2CO_3 , CS_2CO_3 , and $KOtBu$, identified $KOtBu$ as the most efficient base (Table 6, entry 5). Reaction yields improved upon increasing the temperature and extending the reaction time, and, notably, solvent-free conditions resulted in complete conversion with

Table 6 Optimization studies of the *N*-alkylation reaction of aniline with benzyl alcohol catalyzed by complex **3d**^a

Entry	Base	Temperature (°C)	GC yield (conversion A : B%)
1	No base	100	0
2	KOH	100	20.07 (50.73/49.27)
3	K_2CO_3	100	18.9 (58.5/41.5)
4	CS_2CO_3	100	17.36 (67.47/32.53)
5	$KOtBu$	100	24.7 (75.3/24.7)
6	$KOtBu$	120	33.84 (93.0/7.0)
7	$KOtBu$	150	42 (84.72/15.27)
8	$KOtBu^b$	150	67 (92.3/7.7)
9	$KOtBu^c$	150	28.7 (84.66/15.34)
10	$KOtBu^d$	150	0
11	$KOtBu^e$	150	100 (100/0)

^a Reaction conditions: complex **3d** (0.025 mmol, 2.5 mol%), benzyl alcohol (1.5 mmol), aniline (1 mmol), base (1 mmol), toluene (2 mL), and 24 h. The conversions and selectivities were determined by GC analysis, with calibrations based on decane. ^b 36 h. ^c MeOH (2 mL). ^d Without **3d**. ^e Without solvent and for 24 h.



Table 7 Optimization and reproducibility study for the *N*-alkylation reaction using the Pd-PEPPSI catalyst **3d**^a

Entry	Catalyst loading (mol%)	Temperature (°C)	Time (h)	Conversion (%)	Product selectivity (A/B)
1	5.0	100	12	98	100/0
2	2.5	100	12	96	100/0
3	1.0	100	12	88	92/8
4	0.5	100	12	75	85/15
5	2.5	120	24	94	100/0
6	2.5	150	24	100	100/0
7	1.0	150	24	90	95/5
8	0.5	150	24	78	88/12
9	—	150	24	<5	—
10	2.5	150	24	<5	—

^a A = *N*-alkylated amine; B = imine intermediate.

Table 8 *N*-Alkylation of anilines with benzyl alcohols^a

Entry	Amine	Alcohol	GC yield (conversion A: B%)					
			3a	3b	3c	3d	3e	3f
1			100 (82.8/17.2)	99.2 (83.95/16.05)	99.5 (100/0)	99.84 (59.3/40.7)	100 (75.0/25)	97.76 (71.5/28.5)
2			100 (77.0/23.0)	100 (66.9/33.1)	100 (72.0/28.0)	100 (68.8/31.2)	100 (100/0)	100 (83.1/16.9)
3			24 (91.9/8.1)	24 (63.3/36.7)	37.28 (54.2/45.8)	62.7 (23.4/76.6)	35.56 (87.4/12.6)	45.0 (58.4/41.6)
4			52 (96.8/3.2)	63.5 (98.5/1.5)	41 (95.7/5.3)	100 (100/0)	100 (100/0)	100 (100/0)

^a Reaction conditions: complexes **3a–f** (0.025 mmol, 2.5 mol%), benzyl alcohol derivatives (1.5 mmol), aniline derivative (1 mmol), KO^tBu (1 mmol), free solvent, and 24 h. The conversions and selectivities were determined by GC, with calibrations based on decane.

exclusive formation of the amine product (Table 7, entry 11). To address the reproducibility of low catalyst loadings, a clear optimization table is included (Table 7), summarizing the effects of catalyst loading, temperature and reaction time. The data demonstrate that reduced catalyst amounts remain effective and reproducible, with 2.5 mol% identified as the optimal loading under elevated temperature and extended reaction

time. The table provides a systematic comparison of conditions and outcomes, enabling straightforward evaluation of the robustness and reliability of the catalytic system.

The optimized conditions were therefore established as: solvent-free medium, 150 °C, 24 h, KO^tBu as base, and 2.5 mol% catalyst. Using these conditions, the substrate scope of complexes **3a–f** was explored (Table 8). Overall, the catalytic

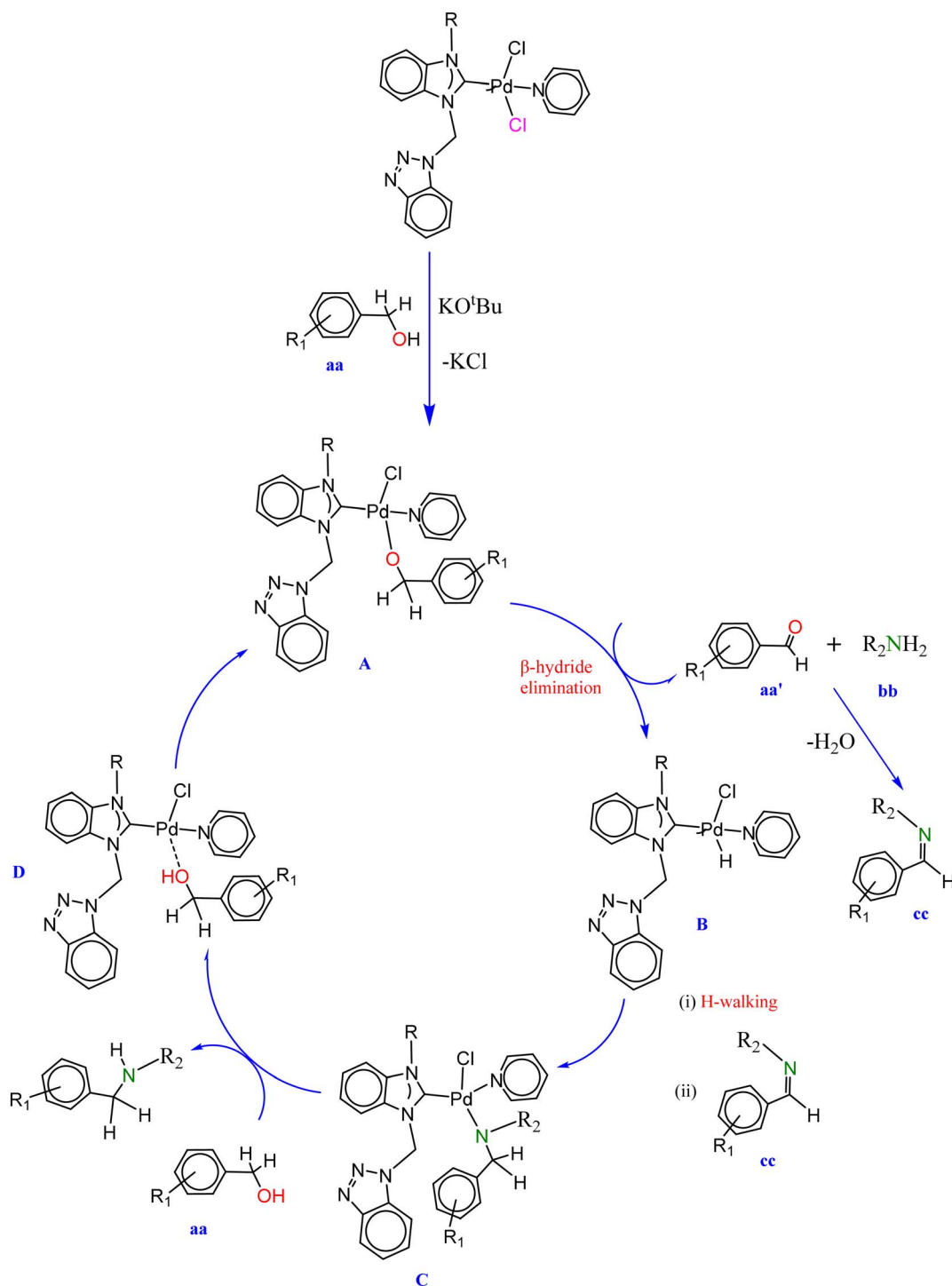
Table 9 Control and benchmarking experiments for the Pd-PEPPSI-catalyzed *N*-alkylation

Entry	Catalyst/Condition	Additive	Conversion (%)	Comment
1	Pd-PEPPSI 3d	—	100	Standard conditions
2	—	—	<5	No catalyst
3	Pd-PEPPSI 3d	Hg(0)	<10	Catalyst poisoning
4	Pd-PEPPSI 3d	Pd-black	<5	Inactive species
5	Pd-PEPPSI-IPr	—	95	Benchmark catalyst



efficiencies of **3a–f** were high, reflecting the structural similarity of the NHC ligands. The *N*-alkylation of pyrrolidine with benzyl alcohol proceeded with high conversion and selectivity, while methoxy-substituted benzyl alcohol achieved 100% conversion with excellent selectivity (Table 8, entry 2). Alkylation of 2,4-dimethylaniline with arylmethyl alcohols also provided high yields of the amine, with only trace amounts of imine, particularly in the presence of electron-donating methyl and methoxy groups (Table 8, entries 3–4).

Interestingly, the steric and electronic properties of the NHC ligands significantly influenced the catalyst performance and selectivity in the present system. Complexes **3d**, **3e**, and **3f**, which feature bulkier or electronically tuned substituents on the benzimidazole ring, exhibited enhanced reactivity and selectivity toward the *N*-alkylated amine, particularly when methoxy-substituted alcohols were used. This suggests that steric hindrance around the palladium center reduces the formation of undesired side products, while electron-donating



Scheme 4 Proposed mechanism for *N*-alkylation catalyzed by NHC-based Pd-PEPSSI complexes **3**.



substituents on the NHC backbone modulate the electron density at Pd, facilitating both alcohol dehydrogenation and imine hydrogenation steps more effectively. Such ligand effects have been widely recognized in borrowing-hydrogen catalysis, where careful design of donor properties and steric bulk can profoundly impact catalytic activity and selectivity.⁵³ For example, recent reviews and studies on borrowing-hydrogen systems report a range of catalysts based on 3d metals, such as manganese, which highlight the importance of ligand architecture in achieving high efficiency and selectivity for C–N bond formation with alcohols.⁵⁴ Similarly, metal–organic–framework supported iridium catalysts demonstrate how ligand and support design can enhance activity and substrate scope in borrowing-hydrogen *N*-alkylation.⁵⁵ In the palladium domain, although Pd-catalyzed borrowing-hydrogen alkylation has been less explored than with Ru or Ir, palladium complexes bearing cooperative ligands have been reported to activate alcohols *via* metal–ligand cooperation, underscoring that ligand electronics and geometry are crucial for catalytic performance.⁵⁶ Compared with these existing catalysts, the present Pd(II)–PEPPSI–NHC complexes exhibit excellent activity and selectivity under solvent-free, mild conditions, even with relatively low catalyst loadings. While borrowing-hydrogen alkylation with alcohols has been widely explored with Ru, Ir, and manganese catalysts,^{57,58} this study represents the first demonstration of borrowing-hydrogen *N*-alkylation using this specific class of Pd–PEPPSI–NHC catalysts, highlighting the potential of rational ligand design in expanding the scope of sustainable amine synthesis.

To further elucidate the nature of the active catalytic species, a series of control and benchmarking experiments was carried out (Table 9). In the absence of the palladium catalyst, no detectable conversion was observed, confirming that the transformation is truly catalyst-dependent. The addition of elemental mercury led to a strong suppression of catalytic activity, while the use of Pd-black as a catalyst resulted in negligible conversion, indicating that inactive palladium aggregates are not responsible for the observed reactivity. These results are consistent with catalysis mediated by molecular palladium species. Furthermore, the catalytic performance of complex **3d** was compared with that of a commercially available Pd–PEPPSI catalyst under identical conditions. Both systems exhibited comparable activity, thereby validating the efficiency and reliability of the synthesized Pd–PEPPSI complex.

Based on the experimental outcomes and literature reports,⁵⁹ we propose a probable mechanism, as shown in Scheme 4. Initially, alcohol is deprotonated by *t*BuOK as a base, which then coordinates to the Pd(II)-center of the catalyst to form the Pd(II)-alkoxy intermediate A. After this, β -hydride elimination occurs, which produces a transient Pd–H intermediate B and a carbonyl species aa'. In the next step, a hydride is transferred from the Pd(II)-center to the azo group of the ligand *via* a hydrogen walking mechanism, and a molecule of alcohol then coordinates to the complex to form intermediate C. After protonation to form the alkoxy intermediate D, an amine intermediate is produced *via* the condensation reaction of the in situ-generated carbonyl compound aa' with an amine cc. The

intermediate D is then hydrogenated by intermediate C to afford the final *N*-alkylated product.

4 Conclusion

In summary, we report the synthesis and the catalytic and biological activities of novel benzimidazolium salts and their corresponding NHC-based Pd–PEPPSI complexes. The newly synthesized benzimidazolium salts, bearing various *N*-substituents and serving as carbene precursors, enabled the preparation of the corresponding NHC-based Pd–PEPPSI complexes through a straightforward synthetic route. The salts and their related Pd–NHC complexes were rationally designed and structurally characterized using spectroscopic and analytical techniques, including NMR (¹H and ¹³C), FT-IR spectroscopy, and elemental analysis. The molecular structure of the novel Pd(II)–NHC PEPPSI-type complex was further confirmed by single-crystal X-ray crystallography. All the newly synthesized complexes were evaluated for their catalytic activity in the alkylation of amines with alcohol derivatives. The results showed that solvent-free conditions afforded higher efficiency and selectivity compared with reactions conducted in a solvent medium, such as toluene, using complexes **3a–f** as catalysts. Furthermore, both electron-donating and electron-withdrawing substituents were well tolerated, providing high conversions. In addition, the antimicrobial activities of the benzimidazolium salts and their Pd(II)–NHC complexes were assessed against bacterial and fungal strains. All Pd(II)–NHC complexes exhibited significant antimicrobial activity against both bacteria and fungi within the concentration range of 50–6.25 $\mu\text{g mL}^{-1}$.

Conflicts of interest

There are no conflicts to declare.

Data availability

CCDC 2521078 contains the supplementary crystallographic data for this paper.⁵⁹

The data supporting this article have been included as part of the supplementary information (SI). Supplementary information is available. See DOI: <https://doi.org/10.1039/d6ra00146g>.

References

- 1 R. Mocchi, L. Atzori, W. Baratta, L. De Luca and A. Porcheddu, *RSC Adv.*, 2023, **13**, 34847–34851.
- 2 N. Joly, S. Gaillard, A. Poater and J. Renaud, *Org. Chem. Front.*, 2024, **11**, 7278–7317.
- 3 M. F. Ansari, A. K. Maurya, A. Kumar and S. Elangovan, *Beilstein J. Org. Chem.*, 2024, **20**, 1111–1166.
- 4 R. Upadhyay and S. K. Maurya, *J. Org. Chem.*, 2023, **88**, 16960–16966.
- 5 P. A. Grieco, *Chem. Rev.*, 2020, **120**, 11401–11471.
- 6 A. Corma, J. Navas and M. J. Sabater, *Chem. Rev.*, 2010, **110**, 1611–1641.



- 7 D. J. Morris, *Top. Organomet. Chem.*, 2013, **43**, 197–234.
- 8 M. A. Cherkasov and A. M. Chusov, *J. Catal.*, 2021, **401**, 1–12.
- 9 E. A. B. Kantchev, C. J. O'Brien and M. G. Organ, *Angew. Chem., Int. Ed.*, 2007, **46**, 2768–2813.
- 10 S. Marion and S. P. Nolan, *Acc. Chem. Res.*, 2008, **41**, 1440–1449.
- 11 I. Özdemir, S. Yaşar, I. Al Nasr, N. Touj, W. Koko and T. Khan, *Catalysts*, 2020, **10**, 1190.
- 12 I. J. S. Fairlamb, *Org. Biomol. Chem.*, 2008, **6**, 3645–3656.
- 13 D. Bourissou, O. Guerret, F. P. Gabbaï and G. Bertrand, *Chem. Rev.*, 2000, **100**, 39–91.
- 14 S. Díez-González, *N-heterocyclic Carbenes*, RSC, 2011.
- 15 P. J. Dyson and F. G. N. Cloke, *J. Organomet. Chem.*, 2022, **965**, 122268.
- 16 S. Werkmeister, K. Junge and M. Beller, *Org. Process Res. Dev.*, 2014, **18**, 289–302.
- 17 M. Chatterjee and S. D. Sarkar, *Chem. Eur J.*, 2021, **27**, 5318–5331.
- 18 R. Grigg and T. R. B. Mitchell, *Synthesis*, 1988, 988–990.
- 19 Y. Watanabe, Y. Tsuji and Y. Ohsugi, *Tetrahedron Lett.*, 1981, **22**, 2667–2670.
- 20 S. Elangovan, A. Spannenberg and H. Jiao, *Angew. Chem., Int. Ed.*, 2021, **60**, 5459–5467.
- 21 P. G. Jessop and X. Qi, *Green Chem.*, 2018, **20**, 92–102.
- 22 G. Guillena, D. J. Ramón and M. Yus, *Chem. Rev.*, 2010, **110**, 1611–1641.
- 23 N. Shimizu, M. Fujita and M. Seki, *ACS Catal.*, 2022, **12**, 10899–10922.
- 24 J. Sun, H. Zhang and A. Narendran, *Catal. Sci. Technol.*, 2021, **11**, 6136–6146.
- 25 Y. Li, A. Mao, X. Hu, L. Wang, D. Wang and Z.-C. Duan, *Dalton Trans.*, 2024, **53**, 5064–5072.
- 26 Y.-S. Chen, S.-Y. Chiu, C.-Y. Li, T.-R. Chen and J.-D. Chen, *RSC Adv.*, 2023, **13**, 31948–31961.
- 27 Y. Guo, J. Zhang, L. He, X.-Y. Zhou, K.-W. Xing and D. J. Young, *Catalysts*, 2024, **14**, 881.
- 28 P. A. Patel, R. Ranjan, N. R. Chauhan, S. Mukhopadhyay, A. R. Choudhury and K. M. Vyas, *New J. Chem.*, 2023, **47**, 8305–8317.
- 29 S. M. Adams, J. R. Stone, P. C. Healy and D. S. Black, *J. Mol. Catal. A: Chem.*, 2022, **421**, 85–96.
- 30 B. Gao, L. Zhang and Q. Li, *ChemCatChem*, 2023, **15**, e202201781.
- 31 S. R. C. A. Gomes, C. L. Souza and L. F. T. Gonçalves, *Catal. Sci. Technol.*, 2024, **14**, 789–802.
- 32 M. A. Abou Ali, *et al.*, *J. Organomet. Chem.*, 2024, **1011**, 123129.
- 33 Y.-S. Chen, *et al.*, *RSC Adv.*, 2023, **13**, 31948–31961.
- 34 W. Chen, M. Sohail and S. T. Madrahimov, *ACS Appl. Mater. Interfaces*, 2025, **17**, 17775–17782.
- 35 S. Elangovan, A. Spannenberg and H. Jiao, *Angew. Chem., Int. Ed.*, 2021, **60**, 5459–5467.
- 36 P. A. Grieco, *Chem. Rev.*, 2020, **120**, 11401–11471.
- 37 M. F. Ansari, A. K. Maurya, A. Kumar and S. Elangovan, *Beilstein J. Org. Chem.*, 2024, **20**, 1111–1166.
- 38 R. Upadhyay and S. K. Maurya, *J. Org. Chem.*, 2023, **88**, 16960–16966.
- 39 (a) M. A. R. Khan, M. A. Islam, K. Biswas, M. Y. Al-Amin, M. S. Ahammed, M. I. N. Manik, K. M. M. Islam, M. A. Kader, A. H. M. K. Alam, S. Zaman and G. Sadik, *Molecules*, 2023, **28**, 793; (b) L. Boubakri, W. Hallab, H. Karci, A. Attour, M. Dündar, İ. Özdemir, N. Gürbüz, A. Koç, İ. Özdemir, H. Naïli, H. Kelm and N. Hamdi, *J. Mol. Struct.*, 2026, 145537.
- 40 N. Sharma, G. Arya, R. M. Kumari, N. Gupta and S. Nimesh, *Bio-protocol*, 2019, **9**, e3131, DOI: [10.21769/BioProtoc.3131](https://doi.org/10.21769/BioProtoc.3131).
- 41 T. Irrgang and R. Kempe, *Chem. Rev.*, 2019, **119**, 2524–2549.
- 42 D. Bensalah, L. Mansour, M. Sauthier, N. Gürbüz, I. Özdemir, W. S. Koko, R. Gatri and N. Hamdi, *New J. Chem.*, 2023, **47**, 20435–20455.
- 43 G. M. Sheldrick, *Acta Crystallogr., Sect. A: Found. Adv.*, 2015, **71**, 3–8.
- 44 G. M. Sheldrick, *SHELXL-2019/1*, Bruker AXS Inc., Madison, WI, USA, 2019.
- 45 M. J. Frisch, G. W. Trucks, H. B. Schlegel, G. E. Scuseria, M. A. Robb, J. R. Cheeseman, G. Scalmani, V. Barone, B. Mennucci, G. A. Petersson, H. Nakatsuji, M. Caricato, X. Li, H. P. Hratchian, A. F. Izmaylov, J. Bloino, G. Zheng, J. L. Sonnenberg, M. Hada, M. Ehara, K. Toyota, R. Fukuda, J. Hasegawa, M. Ishida, T. Nakajima, Y. Honda, O. Kitao, H. Nakai, T. Vreven, J. A. Montgomery Jr, J. E. Peralta, F. Ogliaro, M. Bearpark, J. J. Heyd, E. Brothers, K. N. Kudin, V. N. Staroverov, R. Kobayashi, J. Normand, K. Raghavachari, A. Rendell, J. C. Burant, S. S. Iyengar, J. Tomasi, M. Cossi, N. Rega, J. M. Millam, M. Klene, J. E. Knox, J. B. Cross, V. Bakken, C. Adamo, J. Jaramillo, R. Gomperts, R. E. Stratmann, O. Yazyev, A. J. Austin, R. Cammi, C. Pomelli, J. W. Ochterski, R. L. Martin, K. Morokuma, V. G. Zakrzewski, G. A. Voth, P. Salvador, J. J. Dannenberg, S. Dapprich, A. D. Daniels, O. Farkas, J. B. Foresman, J. V. Ortiz, J. Cioslowski and D. J. Fox, *Gaussian 09, Revision A.1*, Gaussian, Inc., Wallingford, CT, USA, 2009.
- 46 M. A. Spackman and P. G. Byrom, *Chem. Phys. Lett.*, 1997, **267**, 215–220.
- 47 A. Mariconda, F. Grisi, C. Costabile, S. Falcone, V. Bertolasi and P. Longo, *New J. Chem.*, 2014, **38**, 762–769.
- 48 L. Boubakri, S. Yaşar, V. Dorcet, T. Roisnel, C. Bruneau, N. Hamdi and İ. Özdemir, *New J. Chem.*, 2017, **41**, 5105–5113.
- 49 A. W. Salman, G. U. Rehman, N. Abdullah, S. Budagumpi, S. Endud, H. H. Abdallah and W. Y. Wong, *Polyhedron*, 2014, **81**, 499–510.
- 50 D. Chen, N. Özgün, P. Urvil, C. Ferguson, S. M. Dann and T. C. Savidge, *Sci. Adv.*, 2016, **2**, e1501240.
- 51 R. P. Sharma, R. Bala, R. Sharma and P. Venugopalan, *J. Mol. Struct.*, 2004, **694**, 229–234.
- 52 M. B. Bushuev, A. V. Virovets, Y. Garcia, C. Gieck, L. A. Sheludyakova, V. N. Ikorskii, W. Tremel, P. Gütllich and L. G. Lavrenova, *Polyhedron*, 2005, **24**, 797–804.
- 53 G. Guillena, D. J. Ramón and M. Yus, Hydrogen autotransfer in the formation of C–C and C–N bonds, *Chem. Rev.*, 2010, **110**, 1611–1641.



- 54 F. Kallmeier and R. Kempe, Manganese complexes for (de) hydrogenation catalysis, *Angew. Chem., Int. Ed.*, 2018, **57**, 46–60.
- 55 Z. Li, J. Liu, Y. Huang, L. Ma and Z. Li, Metal–organic framework supported iridium catalysts for borrowing-hydrogen N-alkylation of amines with alcohols, *ACS Catal.*, 2018, **8**, 8452–8461.
- 56 C. Gunanathan and D. Milstein, Metal–ligand cooperation by aromatization–dearomatization: a new paradigm in bond activation and catalysis, *Acc. Chem. Res.*, 2011, **44**, 588–602.
- 57 *Topics in Organometallic Chemistry*, ed. J. R. G. de Vries and C. J. Elsevier, The Borrowing Hydrogen Methodology, 2014, Vol. 47, pp. 1–34.
- 58 C. Gunanathan and D. Milstein, Applications of acceptorless dehydrogenation and related transformations in chemical synthesis, *Science*, 2013, **341**, 1229712.
- 59 CCDC 2521078: Experimental Crystal Structure Determination, 2026, DOI: [10.5517/ccdc.csd.cc2qmd3w](https://doi.org/10.5517/ccdc.csd.cc2qmd3w).

